

Article

Multi-Dimensional Data Fusion for Mineral Prospectivity Mapping (MPM) Using Fuzzy-AHP Decision-Making Method, Kodegan-Basiran Region, East Iran

Ali Shabani ¹, Mansour Ziaii ^{1,*}, Mehrdad Solimani Monfared ¹ , Adel Shirazy ²  and Aref Shirazi ^{2,*} 

¹ Faculty of Mining, Petroleum & Geophysics Engineering, Shahrood University of Technology, Shahrood 3619995161, Iran

² Mining Engineering Department, Amirkabir University of Technology (Tehran Polytechnic), Tehran 1591634311, Iran

* Correspondence: mziaii@shahroodut.ac.ir (M.Z.); aref.shirazi@aut.ac.ir (A.S.); Tel.: +98-915-116-4886 (M.Z.)

Abstract: Analyzing and fusing information layers of exploratory parameters is a crucial stride for increasing the accuracy of pinpointing mineral potential zones in the reconnaissance stage of mineral exploration. Remote sensing, geophysical, geochemical, and geology data were analyzed and fused for identify metallic mineralization in the Kodegan-Basiran region (East Iran). Landsat 7 Enhanced Thematic Mapper Plus (ETM⁺), aeromagnetic data, geological data, and geochemical stream sediment samples were utilized. The study area contains some copper indices and mines. Thus, the main focus of this study was identifying the zones with high potential for metallic copper mineralization. A two-stage methodology was implemented in this study: First, extraction of the exploratory parameters related to metallic mineralization and second is data fusion by the hybrid fuzzy-analytic hierarchy process (Fuzzy-AHP) method. Hydrothermal alterations and iron oxides in the area were mapped by applying the optimum index factor (OIF), band ratio (BR), and least squared fit (LS-Fit) to ETM⁺ data. Intrusive masses were positioned as one of the effective parameters in identifying metallic mineralization zones using the gradient tensor method to assess aeromagnetic data. In order to determine the threshold concentration and the location of mineralization anomalies, the K-means clustering algorithm, vertical geochemical zonality (Vz) index, as well as concentration-area (C-A) multi fractal and singularity analysis were implemented on the geochemical data. In conclusion, the potential zones of metallic mineralization in the Kodegan-Basiran region were displayed in a mineral prospectivity map (MPM) derived from the Fuzzy-AHP decision-making method. Finally, to validate the prospectivity map of metallic mineralization, a control area was selected and surveyed by collecting mineralogical, petrological, and stream sediment samples. Field works confirmed the mineralization of Cu and Fe sulfides, oxides, and hydroxides. The high potential areas identified in the MPM can be considered as targets for future Cu exploration in the Kodegan-Basiran area.

Keywords: data fusion; zonality; singularity; K-means clustering; multi fractal analysis; mineral exploration; geochemistry; Iran



Citation: Shabani, A.; Ziaii, M.; Monfared, M.S.; Shirazy, A.; Shirazi, A. Multi-Dimensional Data Fusion for Mineral Prospectivity Mapping (MPM) Using Fuzzy-AHP Decision-Making Method, Kodegan-Basiran Region, East Iran. *Minerals* **2022**, *12*, 1629. <https://doi.org/10.3390/min12121629>

Academic Editors: Mohammad Parsa, Ehsan Farahbakhsh and Rohitash Chandra

Received: 12 November 2022

Accepted: 15 December 2022

Published: 17 December 2022

Publisher's Note: MDPI stays neutral with regard to jurisdictional claims in published maps and institutional affiliations.



Copyright: © 2022 by the authors. Licensee MDPI, Basel, Switzerland. This article is an open access article distributed under the terms and conditions of the Creative Commons Attribution (CC BY) license (<https://creativecommons.org/licenses/by/4.0/>).

1. Introduction

The fusion of information layers with the aim of identifying mineral prospectivity is of great importance, because many parameters play a role in the formation of mineral deposits. Therefore, multi-dimensional data can increase accuracy and precision [1–3]. Remote sensing and geological information are two general groups of data that are used in the identification of mineral prospectivity in the reconnaissance stage [4–8]. Various methods have been used so far to analyze exploratory data in order to identify mineral prospectivity on a reconnaissance scale. The information layers related to remote sensing, geochemistry, geology, and geophysics data are studied by analytical methods and the

desired exploratory parameters are extracted from them (in the form of maps). Then, based on a decision-making method, the final prospectivity map is presented [9–11].

The Kodegan-Basiran area, South Khorasan province is selected for reconnaissance studies of metallic mineralization, which is placed in the metallogenic province of eastern Iran [12]. The study area is located in the Lut geological block, and the evolution of this block has been interpreted as an extensional setting (Figure 1A) [13,14]. In terms of mineral exploration in the Lut block, mineralization of Cu, Pb, Zn, Sb, Hg, and Au have been reported and documented [15,16]. The Eocene–Oligocene volcanics and subvolcanics of the Lut block are related to copper–gold mineralization, including porphyry copper–gold deposits (Khopik, Shadan and Maher Abad), epithermal-type ores (Qaleh Zari, Hired, Shurab, Sehchangi and Howze Rasi), Au–Ag and Pb–Zn–Sb vein-type deposits (Chupan, Khur and Rahi), and magmatic-skarn deposits (Sorkh Kuh and Bisheh), as well as many other sub-economic Tertiary orebodies [15,17–20]. The study area was selected to identify promising targets of future Cu exploration (larger scales) based on regional geological units (Figure 1B) and mineral evidence.

The study area has the potential of metallic mineralization Cu, Au, and Fe. The primary purpose of this research is to investigate airborne geophysics (aeromagnetic data), geochemistry (stream sediment samples), and remote sensing (alterations), along with the lithological, data of the region and their integration to identify metallic prospectivity zones. According to the studies conducted by various researchers in the east of Iran (Sistan structural zone and Lut block), the studied area is a suitable target for metallic mineral prospectivity, especially Cu [21–24].

In present research, remote sensing and aeromagnetic data and field data (i.e., stream sediment samples and host lithology) were used to identify high prospectivity zones of metallic mineralization. Alterations related to metallic mineralization were identified using Landsat-7 (ETM⁺) images. Optimum index factor (OIF) analysis was conducted to separate geological units. Then, the methods of band ratio (BR) and least squared fit (LS-Fit) were used to identify hydrothermal and Fe oxides alterations. Intrusive masses in the area were located by gradient tensor analysis on airborne magnetometric data and considered as an exploratory parameter in the studies. Subsequently based on 1428 geochemical stream sediment samples, vertical geochemical zonality (V_z) index was calculated and geochemical anomaly maps were obtained using the analytical methods of concentration-area (C-A) multi fractal and singularity. To clarify the concentration relationships among supra-mineral elements and sub-mineral elements with particular focus on Cu element, the k-means clustering algorithm was applied on Pb, Zn, Bi, Ag, Cu, and Mo. In the last step, the information layers were integrated using the fuzzy analytic hierarchy process (Fuzzy-AHP) decision method. Fuzzy-AHP as a knowledge-based method that provides intelligent decision based on information layers in the reconnaissance stage [25,26]. The main objectives of this research were: (1) to analyze remote sensing, geophysical, and geochemical information layers; (2) to map prospectivity zones of metallic mineralization based on information layers; (3) to integrate information layers [27] and prepare the final metallic prospectivity map by the fuzzy-AHP method.

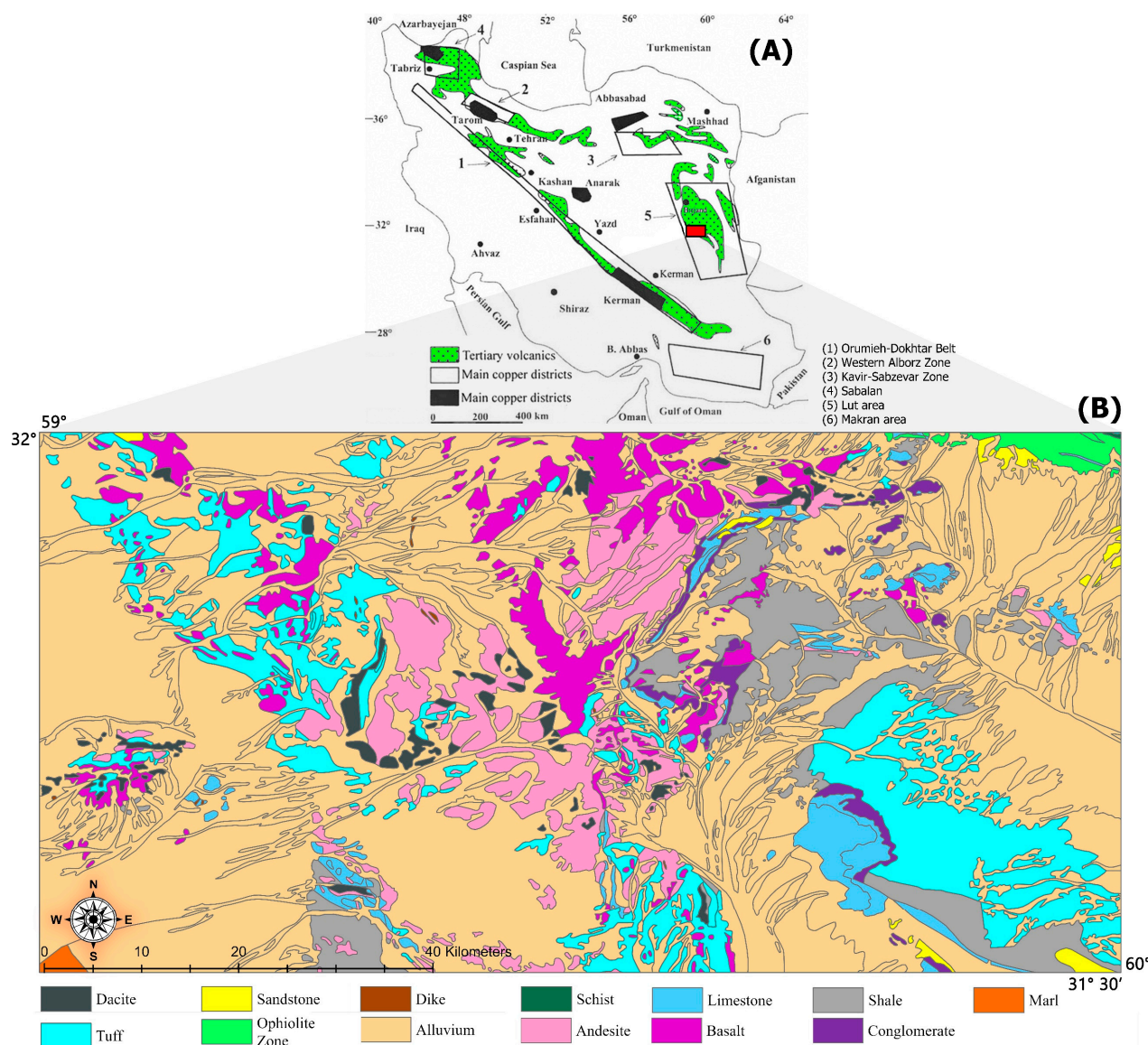


Figure 1. (A) Iran Cu mineralization zones and (B) study area simplified geological map (Combination of Basiran and Kodegan 1:100,000 geological map) [28,29].

2. Geological Setting

The study area (Figure 1) is located at longitude 59° – 60° and latitude 31.30° – 32° in the Sistan structural zone and Lut block in eastern Iran (South Khorasan Province). The most crucial feature of Lut Block, which separates it from other parts of central Iran, is the presence of extensive and massive Tertiary magmatic activity [30,31]. The extensive magmatic activity with unique geochemical characteristics in different parts of the Lut block has caused it to have the potential to form various types of metallic and non-metallic mineralization [28,32,33]. The study area has moderate to acidic intrusive and semi-intrusive rocks that penetrated the Eocene volcanic units. In general, igneous geological units in the study area include andesite, basalt, dacite, ophiolite and tuff [28,29]. The youngest geological unit in the study area is the alluvial sediments of the present age, which in some areas cover the intrusive masses on the surface. In the eastern and southern parts of the area, there is also an extension of the shale unit. The geology of the area includes Cretaceous sedimentary and metamorphosed rocks and Eocene volcanic units that have been intruded by monzonitic to diorite masses of Eocene to Oligocene age. Due to the

intrusion of semi-deep units into highly altered volcanic and carbonate rocks in this area, there is geological potential for metallic mineralization [12,34].

3. Materials and Methods

3.1. Raw Data

3.1.1. Geochemical Sampling

Geochemical sampling of stream sediments in the study area was performed by the Geological Surveys of Iran (GSI). In this sampling, 1428 stream sediment samples (Figure 2) with particle sizes of -80 mesh were collected.

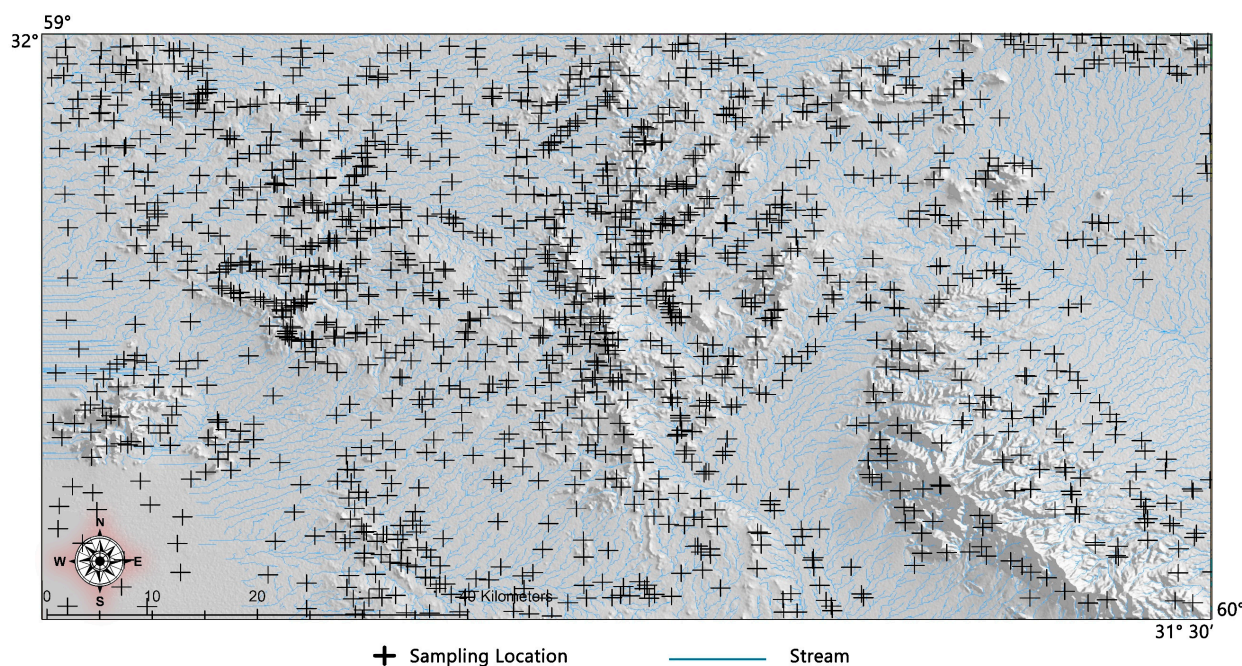


Figure 2. The geochemical sampling network in the study area.

To check the accuracy of the analysis, for every 10–15 geochemical samples, a duplicate sample (about 10% of the total samples) was analyzed. Hence, 110 samples were selected randomly in the study area. Figure 3 shows a diagram of the relative error rate for different elements, where the Au element have a high relative error rate [35]. Finally, the collected samples were analyzed by inductively coupled plasma mass spectrometry (ICP-MS) in the GSI laboratory [35].

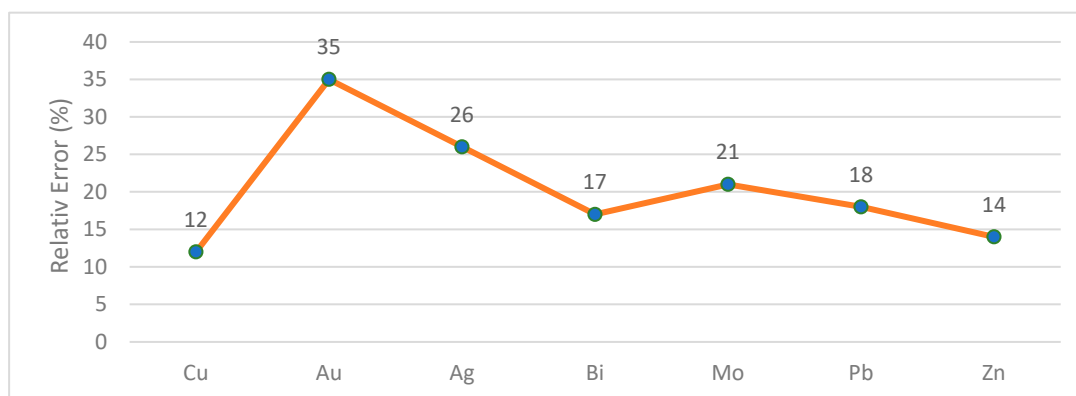


Figure 3. Relative error diagram of duplicate samples in stream sediment analysis [35].

3.1.2. Remote Sensing Data Characteristics and Pre-Processing

Two scenes Landsat-7 (ETM⁺) images of the study area acquired on 15 July 2002 were used. ETM⁺ scenes were obtained from the USGS website (<http://earthexplorer.usgs.gov>). Corrections made on these images include geometric, topographic, and internal average relative reflectance (IARR) atmospheric methods.

3.2. Methodology

Figure 4 presents a flowchart of the methods used in this study. At first, information layers, including (1) remote sensing, (2) geology, (3) geophysics, and (4) geochemistry, were generated using analyzing methods.

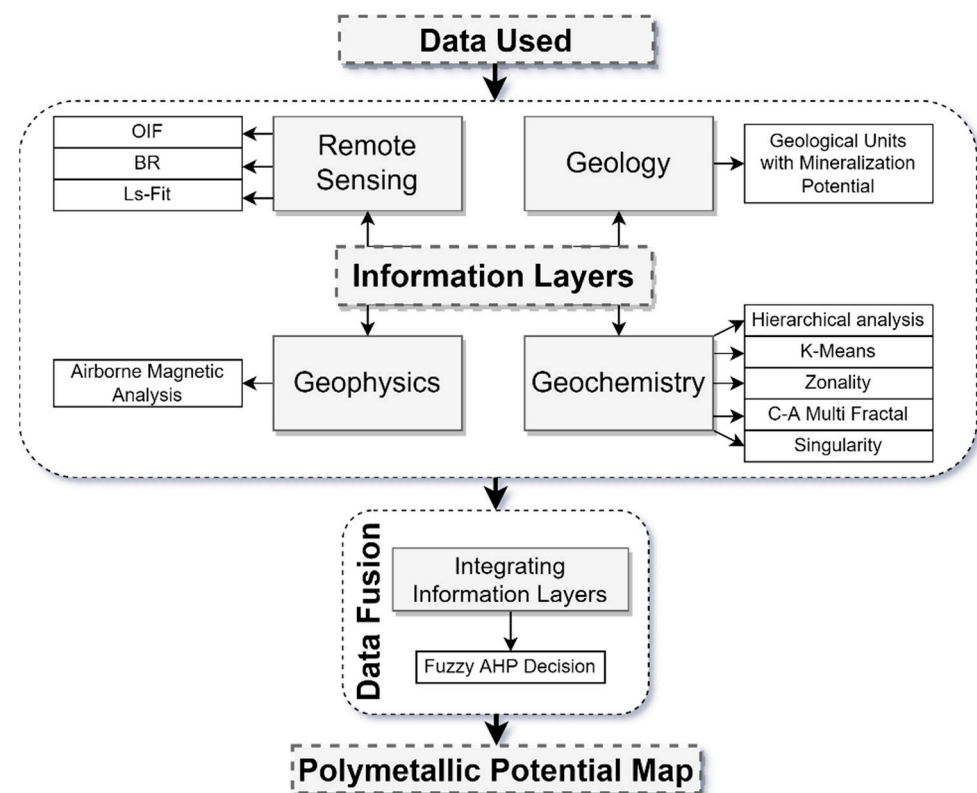


Figure 4. Flowchart of the methodology used in the present study.

Subsequently, in the data fusion stage, all information layers were integrated using the hybrid fuzzy-AHP method [36]. As the final result of the research, a prospectivity map of metallic mineralization was prepared for the studied area.

3.2.1. Remote Sensing Data

In order to process ETM⁺ satellite images in the study area, OIF, BR, and LS-Fit were used. Lithological units were separated by OIF to use in other stages of research such as airborne magnetometric analysis [37]. Alterations related to clay minerals and Fe oxides were identified by the BR method [38,39]. Subsequently LS-Fit analysis was conducted on the satellite image to detect hydrothermal alterations [40]. All the remote sensing methods that have been used in the research produce maps to identify the exploratory parameters of metallic mineralization prospectivity in the study area.

3.2.2. Geophysical Data

The gradient tensor method was used to investigate airborne magnetic data of the study area. The aim of using magnetometric data analysis is to estimate the trend and situation of igneous masses. Subsequently, in order to find the metallic mineralization

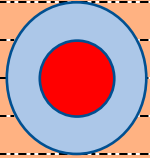
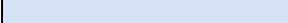
prospectivity, the relationship between igneous masses and regional geology was investigated. Among the various methods which use gradient analysis to estimate the situation of igneous masses, the gradient tensor method uses horizontal gradients and vertical gradients simultaneously (dx, dy and dz). This method can generate more accurate results in estimating the borderline of magnetic anomalies [24,41]. In this study, a residual magnetic map was prepared using gradient tensor method and the igneous masses related to magnetic anomalies were investigated.

3.2.3. Geochemical Data

(A) Zonality Method

The primary halos of ore deposit are made up of different parts of the ore, including host rock and main elements of the deposit [42]. Primary geochemical halos of mineral deposits, which result from the impact of hydrothermal fluids on bedrock, are characterized by the enrichment or depletion of desired elements. Therefore, these geochemical halos are valuable guides for mineral prospecting. The vertical geochemical zonality (V_z) index, which is obtained based on the Supra/Sub mineral elements, are applicable for prospectivity mapping [43]. V_z index shows the mineralization level and its primary geochemical haloes. Ziaii (1996) [44] presented a model for identifying the erosional surface of copper porphyry deposits by three types of V_z indexes (V_{z1} , V_{z2} , and V_{z3}) in Table 1 [44]. The V_z indices based on sub/supra mineral elements show the mineralization phase and the primary halos. Ziaii (1996) [44] invented a model to calculate the mineralization phase in triple V_z [44,45].

Table 1. The types of V_z index for identifying the erosional surface of Cu porphyry deposits (deposits from Iran, Kazakhstan, Armenia and Bulgaria) [44].

Erosional Surface	No	Vertical Section Contrast $V_z(I)/V_z(VI)$	$V_{z1} = \frac{Zn * Pb}{Cu * Ag}$	$V_{z2} = \frac{Zn * Pb}{Cu * Mo}$	$V_{z3} = \frac{Zn * Pb * Bi}{Cu * Ag * Mo}$
			Supra-Ore	I	
Upper-Ore	II		100–10	5–0.5	1–0.1
Ore	III		10–1	0.5–0.05	0.0–0.01
Ore	IV		1–0.1	0.05–0.005	0.001–0.0001
Lower Ore	V		0.1–0.01	0.005–0.0005	0.001–0.0001
Sub-Ore	VI		<0.01	<0.0005	<0.0001
LEGEND			Ground Surface		Ore Body
		Enclosing Rocks		Primary Halo	

(B) K-means Clustering Method

In order to group the geochemical elements into clusters (based on common characteristics), the K-means clustering method was used [46]. The center of clusters was used in the investigations instead of analyzing large numbers of data. The five main steps of the K-means algorithm are given below [47]:

- (1) The number of K is chosen randomly, and all members are divided into K clusters.
- (2) The Z_j vector is calculated by Formula (1). In the presented equation, C_j is the class center value.

$$z_j = \frac{\sum_{x \in C_j} x}{\#C_j} \quad j = 1 \dots k \tag{1}$$

- (3) Formula (2) is the calculator of the considered clusters.
 X : the vector of C_j members; $\#C_j$: The number of C_j members [48].

- (4) Formula (2) calculates the objective function, from which the distance of members from the centers is determined.

$$f(C_1.C_2.\dots.C_k) = \sum_{j=1}^k \sum_{X \in C_j} |X - z_j|^2 \quad (2)$$

- (5) Finally, the optimal number of clusters (K) is provided according to the minimum objective function.

Shirazi et al. [49] introduce software to quickly performs the above algorithm [48,50]. The purpose of using the K-means clustering method is to model the concentration changes of supra-mineral elements and sub-mineral elements versus Cu.

(C) Concentration-Area (C-A) Fractal Method

The principles of Euclid's geometry are not followed by some rare irregular shapes. Fractal geometry is the name given to the geometry that describes these phenomena. Fractal and multi-fractal analysis apply to geochemical and geological investigations. The spatial distribution and shape of the anomalies can be studied by fractal methods.

Chen et al. [51] presented various methods of using fractal analysis to separate geochemical communities. The concentration of fractal properties is given below: An equation is presented below for the concentration of materials or fractal properties:

$$A(\geq v) \propto v^{-\alpha} \quad (3)$$

where $A(\geq v)$ shows the cumulative area surrounded by contour lines (whose related concentration is greater than or equal to v). The α value is the fractal dimension of the different amplitudes [52,53]. The purpose of using the C-A fractal method in the present research was to find the geochemical thresholds of supra-mineral and sub-mineral elements communities.

(D) Singularity Method

The singularity method determines geochemical anomalies with soft threshold form [54]. This method uses local thresholds and some window-based contrast singularity maps [55,56]. Singularity analysis is suitable for use relying on continuous sampling to define anomalies where metals in rock deposits have a Pareto tail [57,58]. The singularity of the element is obtained from the average concentration of $C(A)$ at different A by the Ls-Fit of a straight line on the log-log sheet. Singularity equations can be found as Equations (4) and (5):

$$C(A) = cA^{\alpha/2-1} \quad (4)$$

$$\log C[A(r_i)] = C_0 + (\alpha - 2) \log (r_i) \quad (5)$$

where $C(A)$ shows the concentration of the A area with size of r_i , the C and C_0 are constant values and the α is the relationship exponent. In Equation (4), $\log (C)$ Vs. $\log (r_i)$ is a line where C_0 is y-intercept, and its slope is $\Delta\alpha = \alpha - 2$. The negative slope of line ($\Delta\alpha < 0$) shows the elements enrichment and counter. Therefore, areas with singularity index less than 2 ($\alpha < 2$) indicate concentration enrichment [59].

3.2.4. Data Fusion

(A) Hybrid Fuzzy-Analytic Hierarchy Process (Fuzzy-AHP) method

The fuzzy-AHP method was conducted as a knowledge-based method to create an integrated metallic prospectivity map in the study area. In fact, the fuzzy-AHP is a decision-making method based on priorities [60–62]. Each of the information layers, including maps of geology, geochemistry, airborne magnetometry, and remote sensing are weighted. Subsequently, based on the assigned weights, all the fuzzified layers are integrated. Finally, the prospectivity map of the metallic mineralization is obtained. In general, the process used consists of four principles [26,63]: (i) determining the main-criteria and sub-criteria of

the decision; (ii) calculating the weights of main-criteria and sub-criteria; (iii) fuzzification stage: all information layers are fuzzified; and (iv) final stage: integration of information layers based on calculated weights of main-criteria and sub-criteria.

4. Analysis and Results

4.1. Remote Sensing Analysis on ETM⁺ Satellite Image

4.1.1. Optimum Index Factor (OIF) Analysis

The OIF method was applied to ETM⁺ image in order to separate geological units. After applying the OIF on different bands of the ETM⁺ satellite sensor, the combination of RGB bands 5-3-1 has the highest optimal index factor. In fact, it can be said that the histogram of these three selected bands has the lowest correlation and the most information can be extracted from it [64]. Figure 5 shows the result of the OIF analysis on the ETM⁺ satellite image. As can be seen, the geological units were separated well, in agreement with the trust geology of the area.

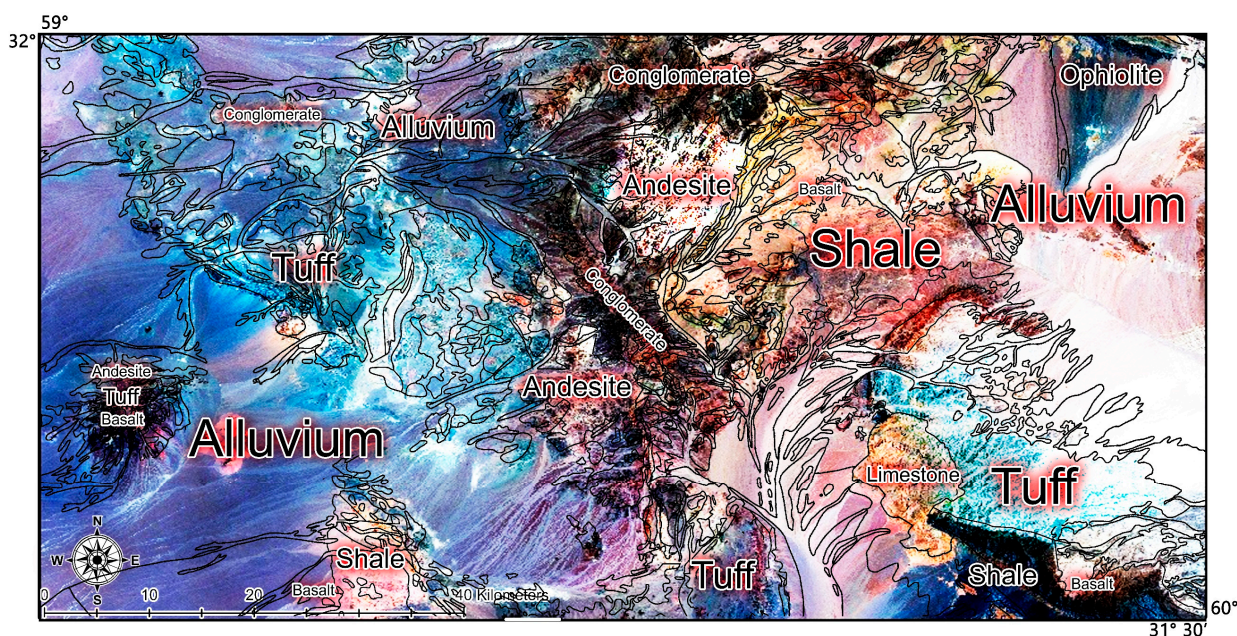


Figure 5. The resulting image from the RGB band composition of 5-3-1 on the ETM⁺ satellite sensor was determined by the OIF.

4.1.2. Band Ratio (BR) Analysis

In order to identify iron oxide areas, the band ratio of 3/1 was applied, and to highlight areas with the most clay minerals the band ratio of 5/7 was used. Finally, the combination of RGB bands = 5/7, 3/4, 3/1 was prepared in Figure 6 to better highlight Fe oxides (pale blue) and minerals including hydroxyl (pink).

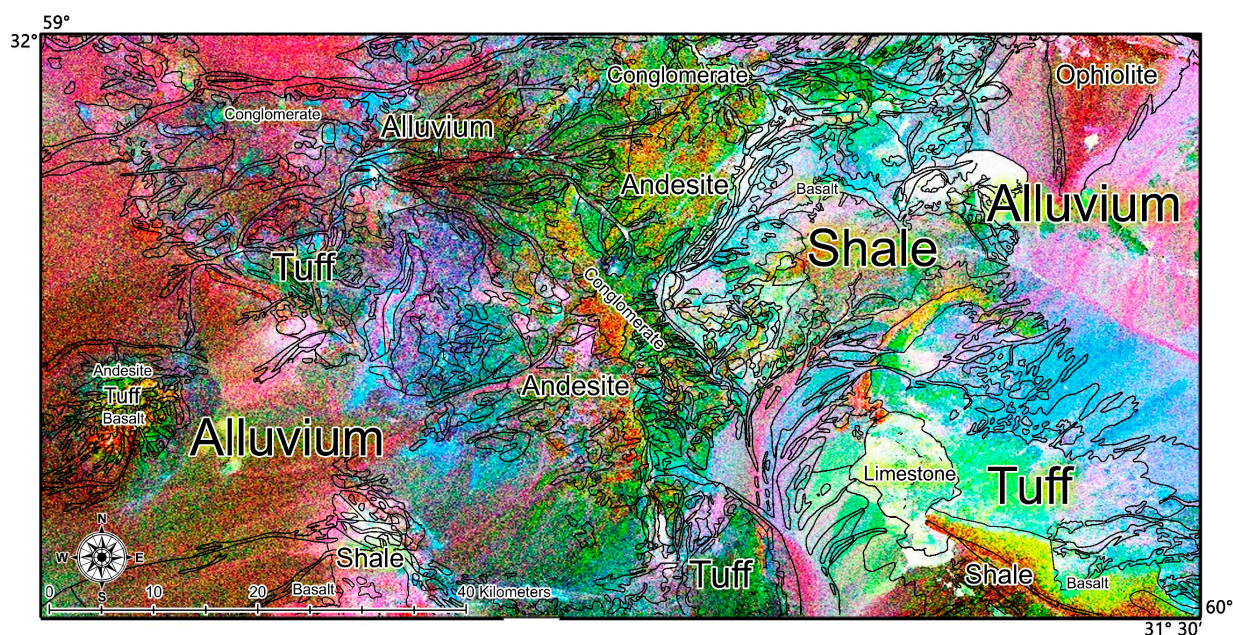


Figure 6. The image resulting from the band ratio combination (RGB = 5/7, 3/4, 3/1) on the ETM⁺ satellite sensor.

4.1.3. Least Squares Fit (LS-Fit) Analysis

In ETM⁺ satellite sensor data, band 7 for hydrothermal alterations and band 3 for Fe oxides were selected. As a result, to prepare a false color combination (RGB), the inverse residue of band 7 ($-R7$), the residue of band 4 ($R4$), and the residue of band 3 ($R3$) were used. In Figure 7, pink and blue pixels represent argillic and propylitic alterations, respectively.

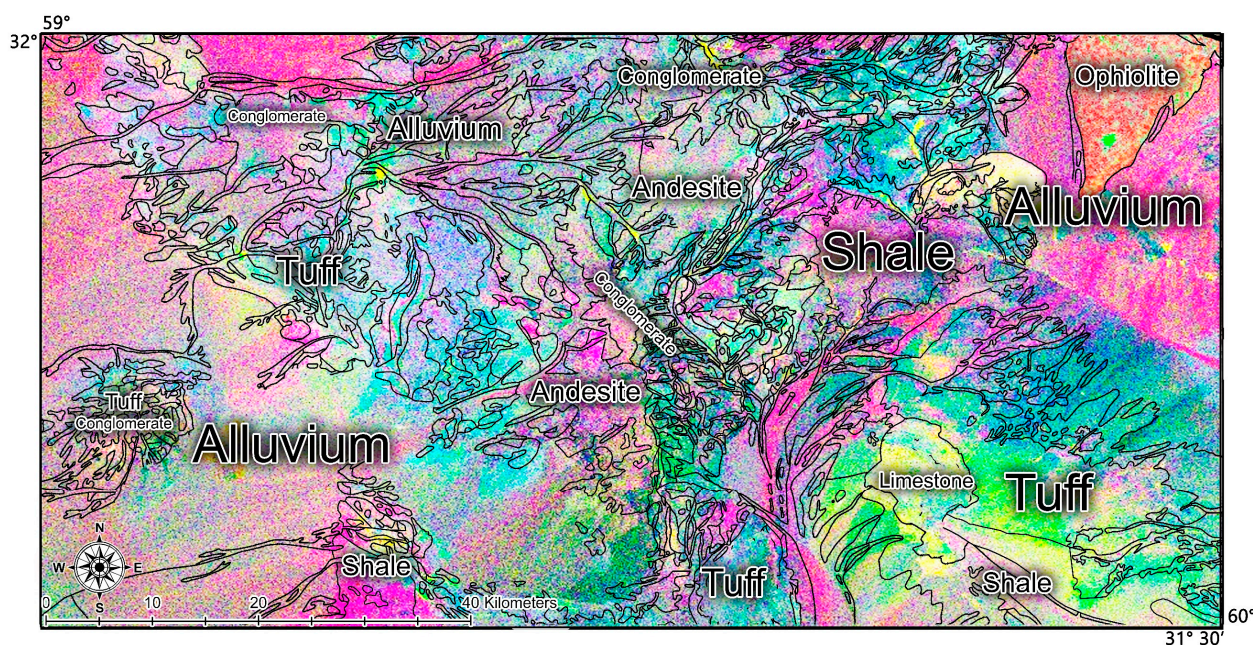


Figure 7. The image resulting from the false color combination of $-R7$, $R4$ and $R3$ residues (RGB = $-R7$, $R4$, $R3$) using the Ls-Fit method from the ETM⁺ satellite sensor.

4.2. Airborne Magnetometric Data Analysis

As can be seen in the remaining map presented in Figure 8, on the eastern side of the area, a sharp dipole can be seen, which is currently covered with alluvium deposits.

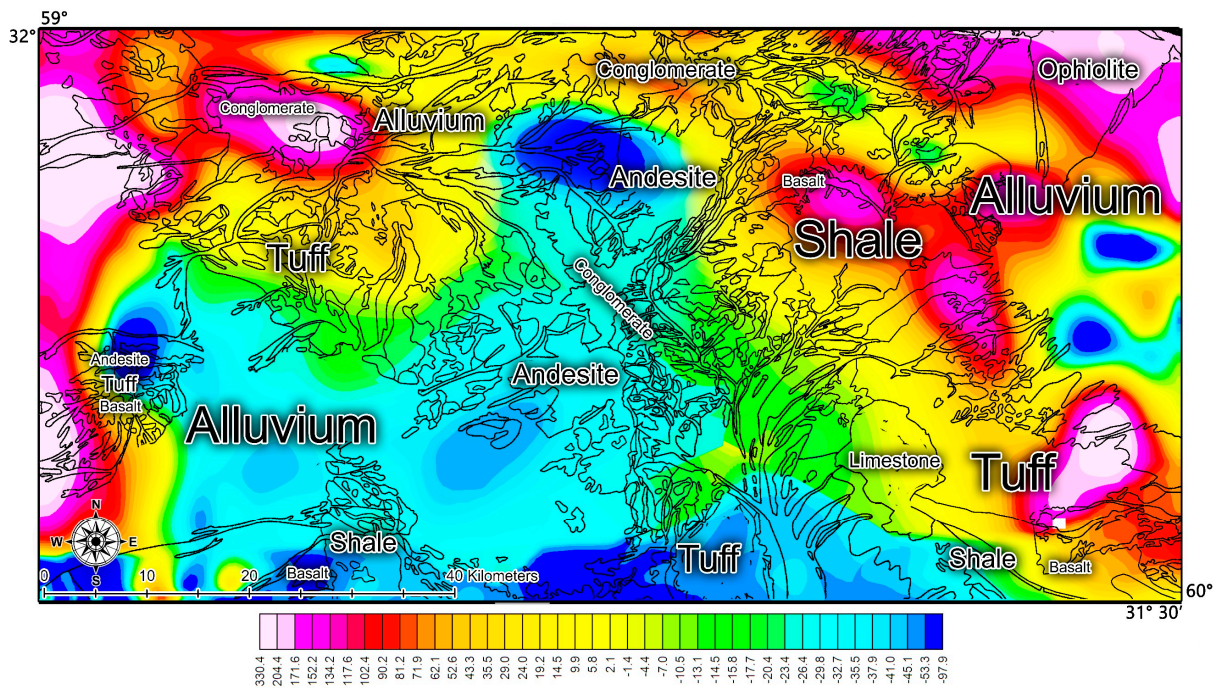


Figure 8. The residual map of airborne magnetometric data analyzed by gradient tensor method.

Based on the results of remote sensing, the eastern part of the area has been identified as Fe oxide areas, so this dipole can be considered in connection with possible Fe mineralization. Negative monopoles are evident in the central areas which can be related to metallic sulfide mineralization according to the distribution of hydrothermal alterations. In the western part (to the southwest) of the area, another bipolar can be seen. According to the geological map and the results of the alteration identification, it is related to basalt, andesite, and dacite masses.

4.3. The Predictor Composition of Cu Mineralization

The descriptive statistical parameters of Cu, Mo, Pb, Zn, Ag, Au, and Bi elements are presented in Table 2. Ziaii et al. investigated four porphyry copper mines, including Aktogay (Kazakhstan), Teghut (Armenia), Assarel (Bulgaria), and Sungun (Iran). Based on this research, the Pb, Zn, and Bi elements are located in the supra-mineral halos and the elements of Cu, Ag, and Mo are located in the sub-mineral halos [44,65].

Table 2. Descriptive statistical parameters of Cu, Au, Ag, Bi, Mo, Pb and Zn based on 1428 geochemical stream sediment samples (Raw Data).

Elements	Cu	Au	Ag	Bi	Mo	Pb	Zn
Mean (ppm)	38.88	2.53	0.16	0.85	1.27	19.15	107.75
Median (ppm)	38.84	1.10	0.13	0.30	1.15	15.40	98.57
Mode (ppm)	17.30	1.00	0.05	0.30	1.35	17.00	74.00
Std. Deviation (ppm)	69.35	25.10	0.51	4.00	2.26	27.28	44.03
Variance (ppm ²)	4809.79	629.84	0.26	15.96	5.10	744.27	1938.20
Skewness	21.15	25.19	21.92	9.18	29.14	13.03	2.78
Kurtosis	500.87	659.82	523.89	95.78	987.58	204.39	21.20
Range (ppm)	1738.28	702.95	13.37	57.03	78.70	520.29	588.89
Minimum (ppm)	0.15	0.30	0.01	0.10	0.30	0.15	0.15
Maximum (ppm)	1738.43	703.25	13.38	57.13	79.00	520.44	589.04

The raw geochemical data were pre-processed in order to use them in the statistical methods. In the first step, the outlier data were identified by the box-plot method and

replaced with the values of the highest and lowest data. Moreover, according to the available raw data, no censored data were reported. In the next step, the data were evaluated as a lognormal distribution. Therefore, the data were normally distributed by the logarithmic method.

Hierarchical Clustering Analysis (HCA)

HCA diagrams regarding the elements Ag, Au, Zn, Pb, Mo, Sn, and Cu were established. As shown in Figure 9, the direct relationship diagram shows Ag, Cu, and Mo as one branch and Bi, Zn, Pb, and Au as another branch.

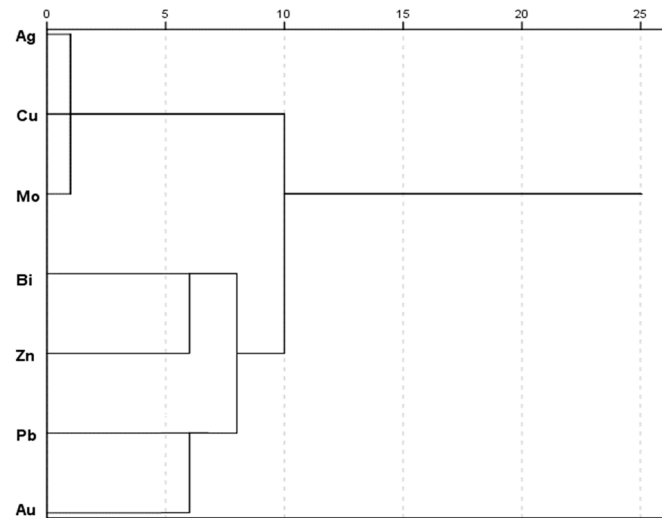


Figure 9. The result of Hierarchical Clustering Analysis (HCA) of data in the form of a dendrogram.

4.4. K-Means Clustering

The concentration relationship of Cu element with the elements of Au, Ag, Mo, Pb, Zn, and Bi was investigated using the K-means clustering method. To identify the optimal number of clusters in the K-mean clustering, the K number was increased from 3 to 10. Figure 10 shows the value of the utility function against the number of clusters for all elements in the same group as the Cu element. Finally, the behavior of Cu versus mentioned elements is modeled according to the diagrams below (Figure 10).

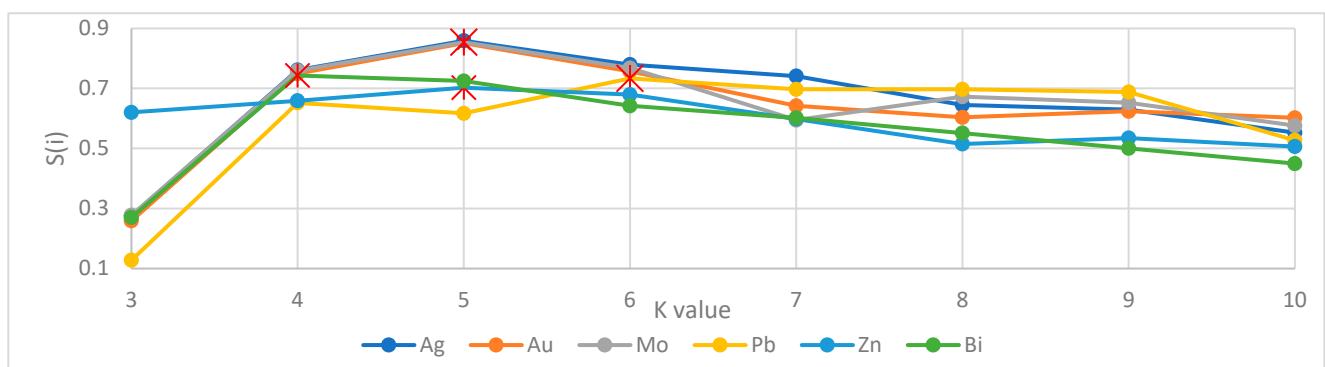


Figure 10. A graph of the utility function S (i) value versus the number of clusters for the Cu versus Ag, Au, Mo, Pb, Zn and Bi.

Based on Figure 10, the number of five clusters is the optimal number of clusters for the behavior of copper element compared to Ag, Au, Mo, and Zn elements, with six clusters for Pb and four clusters for Bi element (Figures 11 and 12).

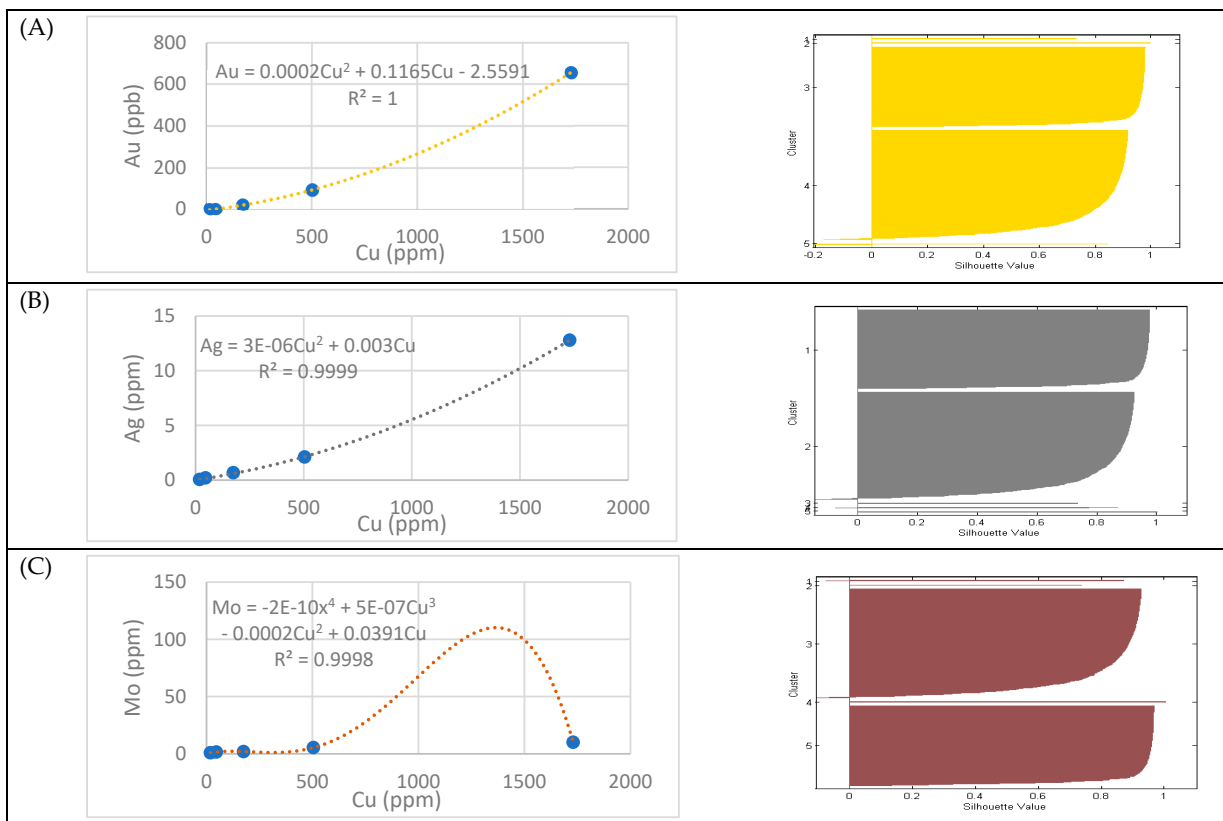


Figure 11. The profile of the clusters and the behavior of Cu and Au, Ag, Mo and concentrations in the centers of clusters. (A) Au-Cu, (B) Ag-Cu, (C) Mo-Cu.

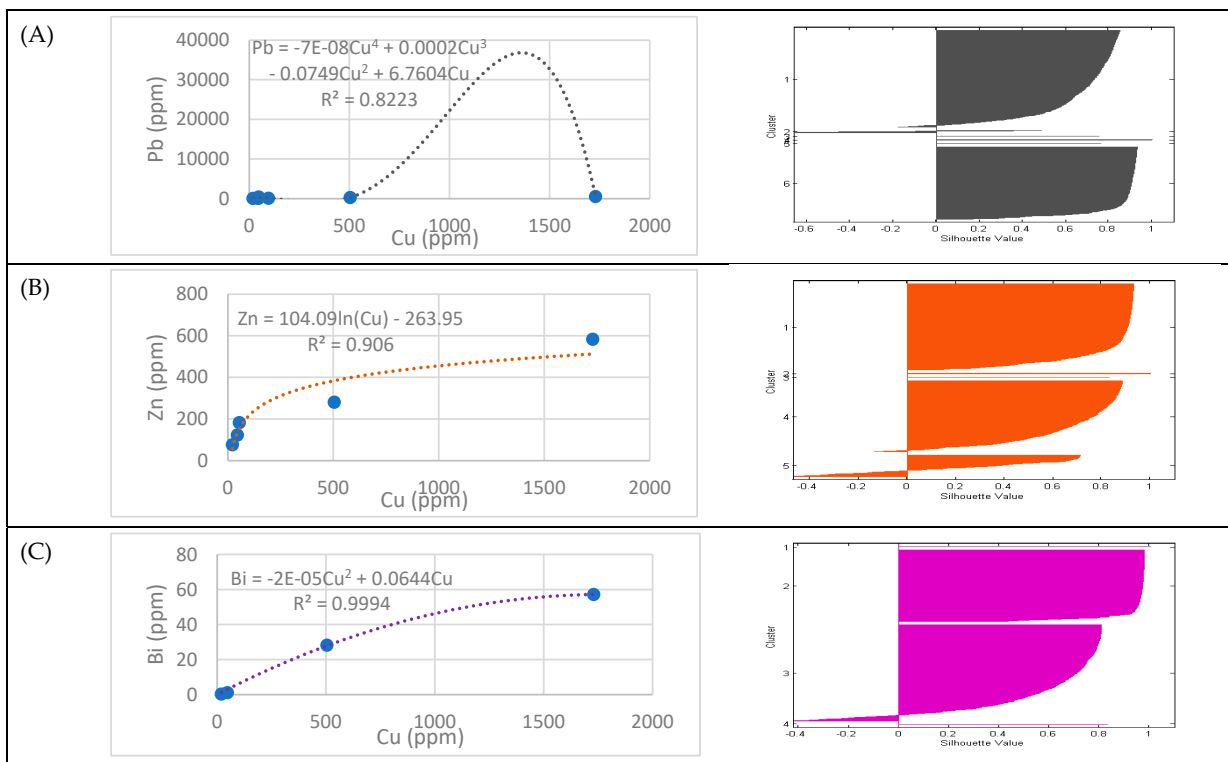


Figure 12. The profile of the clusters and the behavior of Cu and Pb, Zn and Bi concentrations in the centers of clusters. (A) Pb-Cu, (B) Zn-Cu, (C) Bi-Cu.

4.5. Geochemical Exploration by $G(V_{z3})$ Model

The distribution maps of supra-mineral elements (Pb, Zn, Bi) and sub-mineral elements (Cu, Ag, Mo) based on stream sediment samples were prepared, as shown in Figures 13 and 14, respectively. These distribution maps were prepared using the IDW interpolation method. In order to standardize the map, logarithmic data were used in the preparation of the maps.

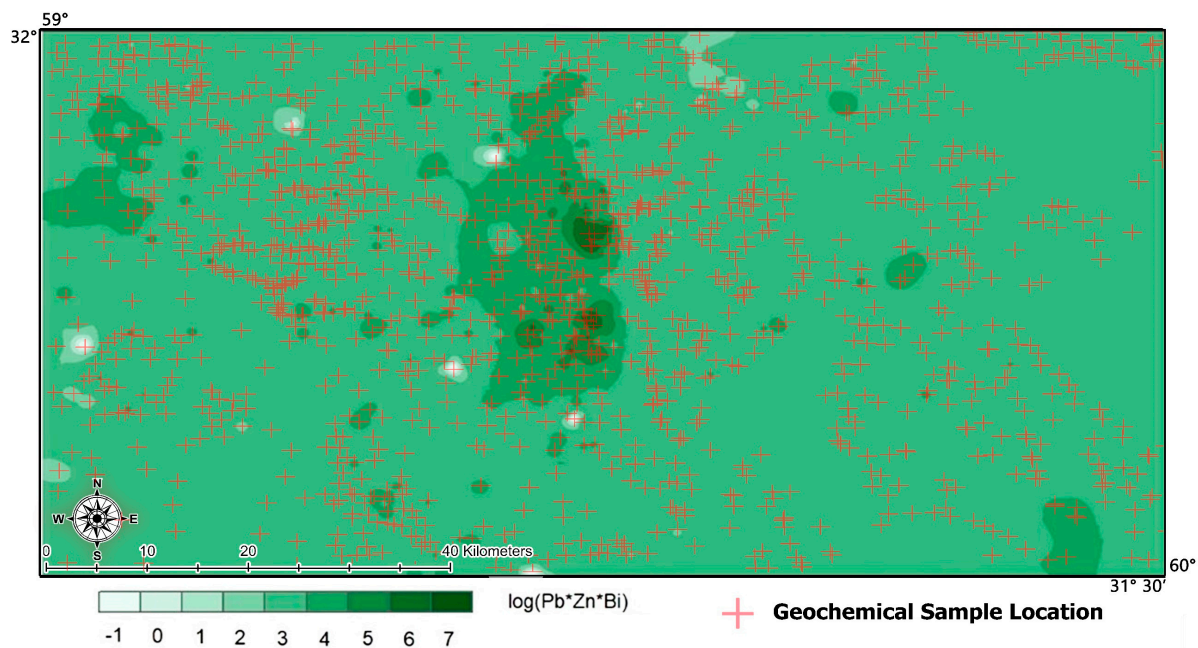


Figure 13. The map of supra-mineral elements distribution based on stream sediment samples (using the IDW interpolation method).

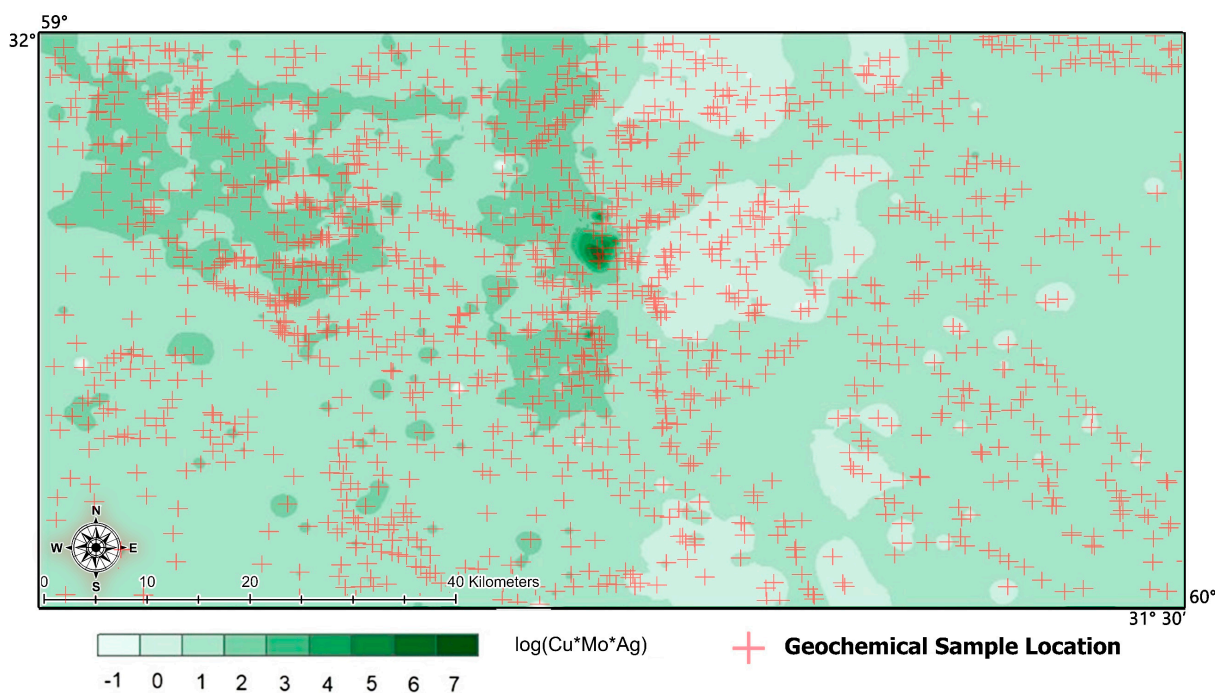


Figure 14. The map of sub-mineral elements distribution based on stream sediment samples (using IDW interpolation method).

In the areas with Cu, Mo, and Ag mineralization, if the supra-mineral elements are depleted, the probability of erosion of the porphyry reserve is high [44]. For this purpose, a distribution map of the sub-mineral elements is needed.

4.6. Concentration-Area (C-A) Multifractal Analysis

In order to determine the threshold limit of the geochemical anomalies in the study area, the C-A multifractal method was used. Figure 15 shows the multifractal diagram related to the supra-mineral elements map presented in Figure 16.

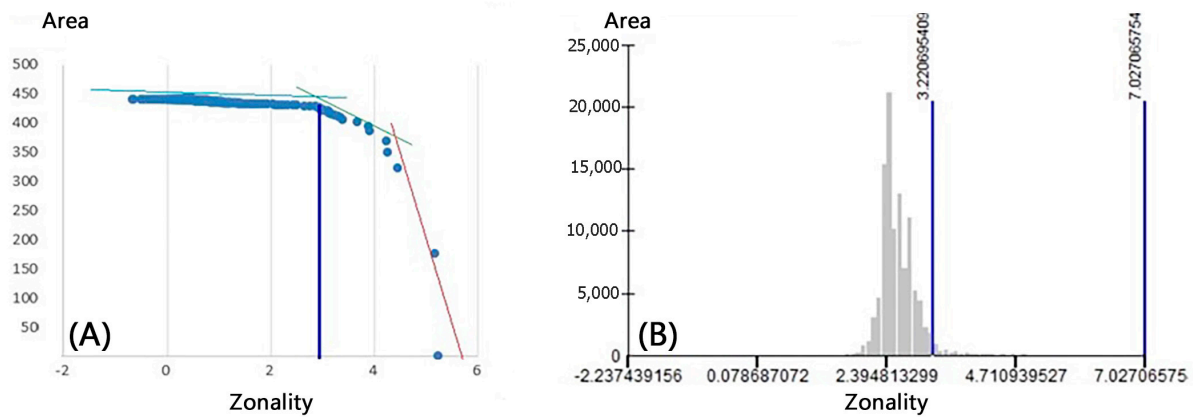


Figure 15. (A) Multifractal diagram of supra-mineral elements (Log(Pb*Zn*Bi) versus Log (area) for stream sediment samples); (B) Histogram of the calculated areas.

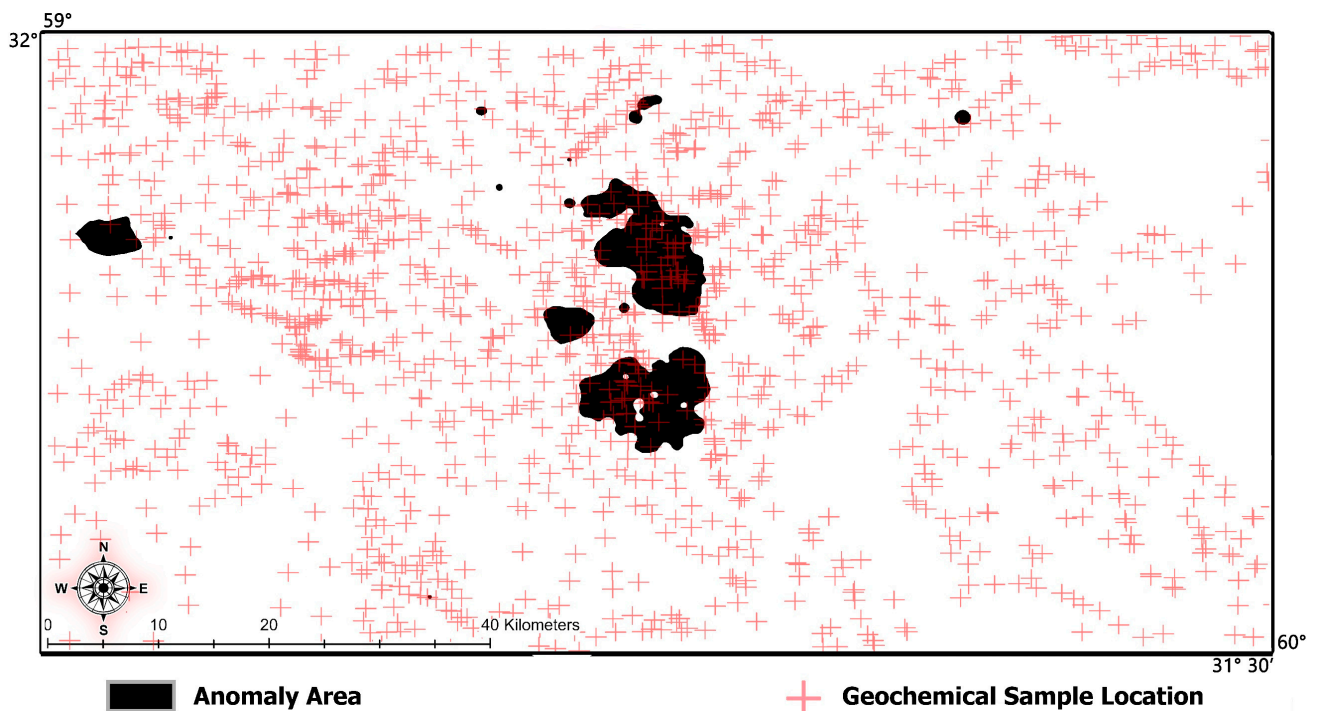


Figure 16. The prospectivity map of supra-mineral elements based on stream sediment samples.

Based on Figure 14, the supra-mineral index and fractal dimensions of the model were obtained, and the threshold limit of the geochemical communities was determined, which is shown in Table 3.

Table 3. Geochemical communities of Supra-mineral elements (Pb*Zn*Bi) based on C-A multifractal analysis.

Geochemical Communities	Threshold Limit of Supra-Mineral Elements (Pb*Zn*Bi)
Background	$Pb*Zn*Bi < 1584$
Anomaly	$1584 < Pb*Zn*Bi < 14,850$
Enrichment	$Pb*Zn*Bi \leq 14,850$

The map presented in Figure 15 shows the anomalous areas of supra-mineral elements in the studied area.

In the following, fractal analysis was also applied to the distribution map of the sub-mineral elements in order to determine the geochemical threshold limits. The results are presented in Figure 17 and Table 4.

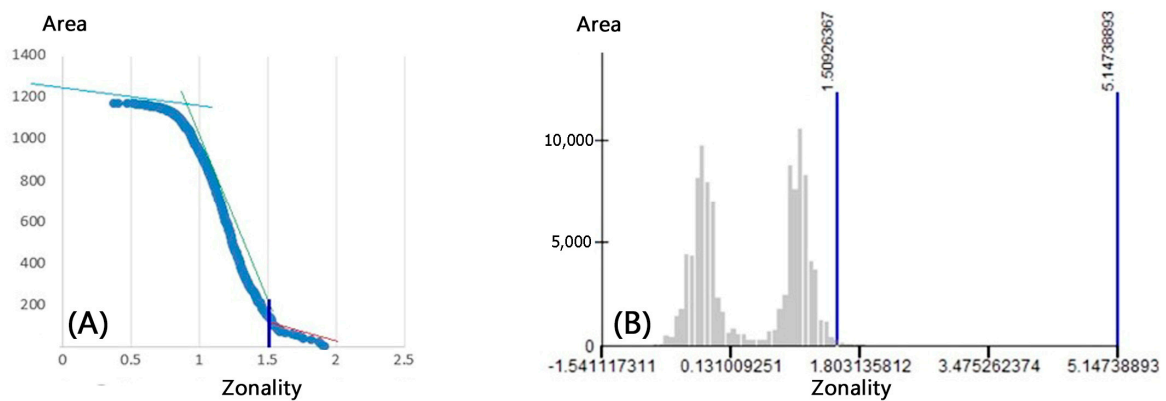


Figure 17. (A) Multifractal diagram of sub-mineral elements (Log (Ag*Cu*Mo) versus Log (area) for stream sediment samples); (B) Histogram of the calculated areas.

According to the threshold limits of geochemical communities for sub-mineral elements, a map of the anomaly community is shown in Figure 18.

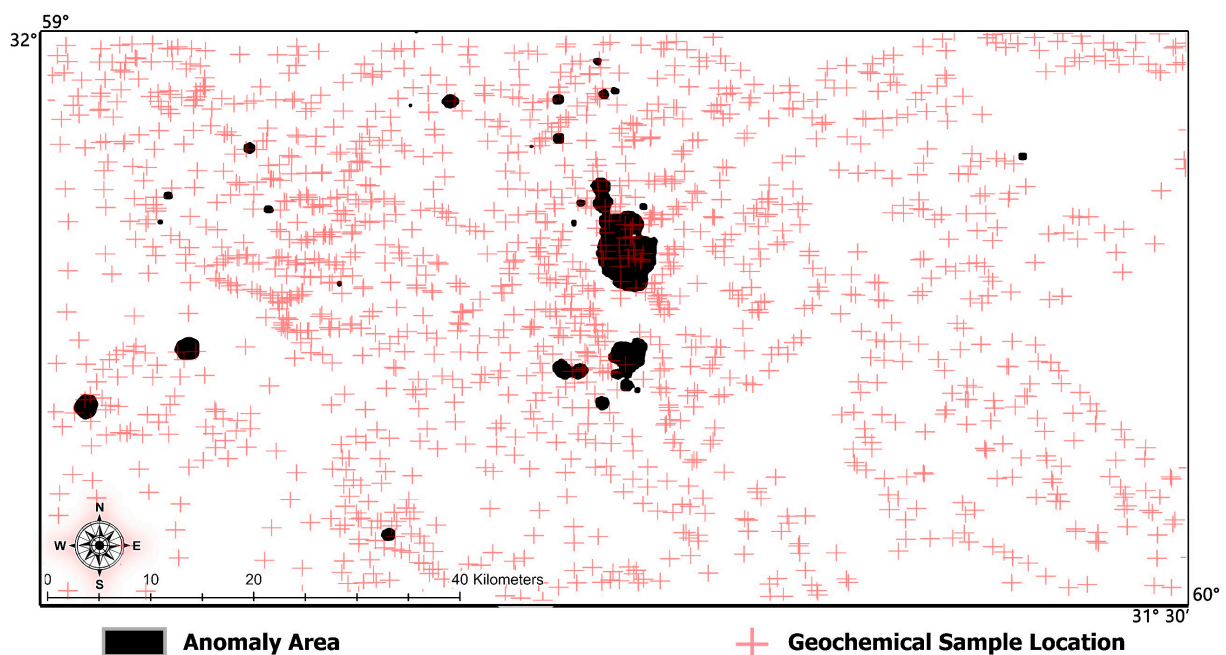


Figure 18. The map of the anomaly community.

Table 4. Geochemical threshold limits of sub-mineral elements based on C-A multifractal analysis.

Geochemical Communities	Threshold Limit of Sub-Mineral Elements (Ag*Cu*Mo)
Background	$Cu*Mo*Ag < 6.3$
Anomaly	$6.3 < Cu*Mo*Ag < 31$
Enrichment	$Cu*Mo*Ag \leq 31$

4.7. Singularity Analysis

According to the singularity method applied to the zonality index in the study area, the singularity map of zonality index is provided in Figure 19.

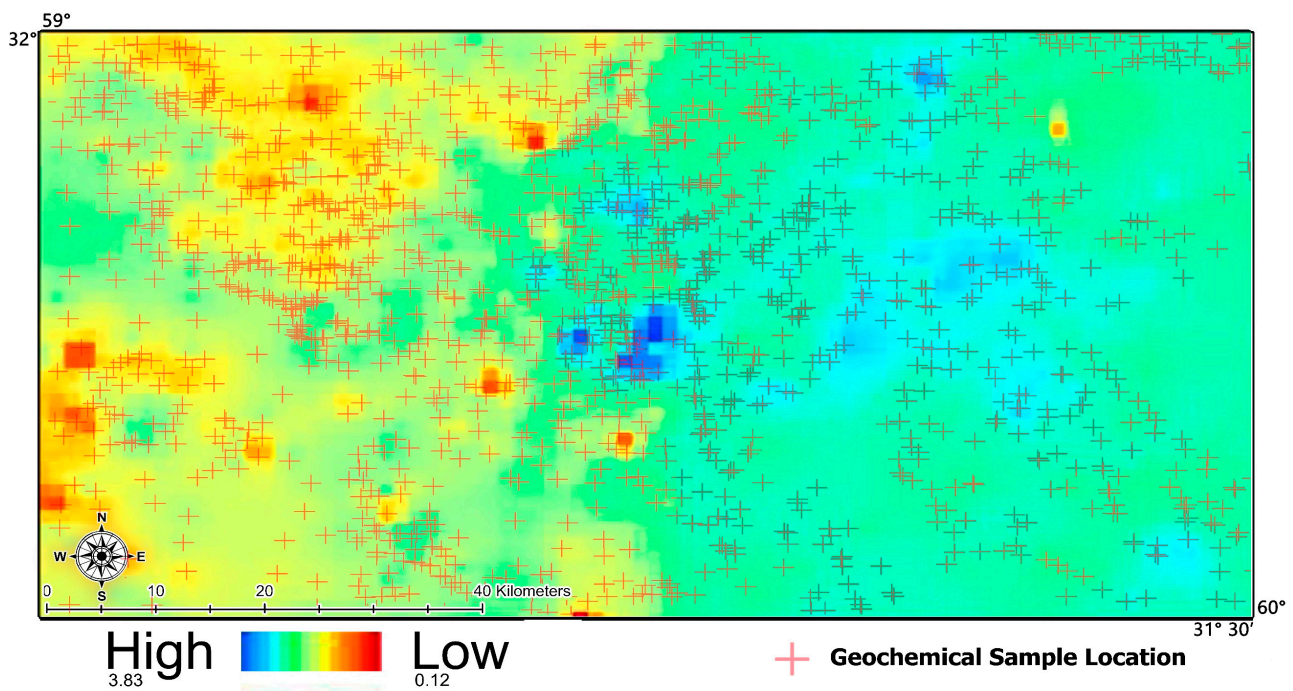


Figure 19. Singularity map of zonality index— $(Pb*Zn*Bi)/(Cu*Mo*Ag)$.

The sampling network was weighted in 1 km² pixels and singularity values greater than two were considered as metallic prospectivity anomaly.

4.8. Hybrid Fuzzy-Analytic Hierarchy Process (Fuzzy-AHP) Method

The information layers that have been investigated so far regarding metallic prospecting in the area are: (1) geology; (2) geochemistry; (3) alterations; and (4) geophysics. In fact, the main decision criteria of the fuzzy-AHP method are these layers. The hierarchical diagram of the criteria and sub-criteria used in the hybrid fuzzy-AHP method is presented in Figure 20.

Each criterion and sub-criterion considered in the integration process should be weighted. This weighting is based on expert opinions supported by many metallic studies in the east of Iran [24,25,36,66–71] as well as the priority table [72,73]. The information related to the weighting of the main criteria and sub-criteria are shown in Table 5. It should be noted that the value of CR for all prioritizations was less than 0.1%, which indicates the appropriateness of the results.

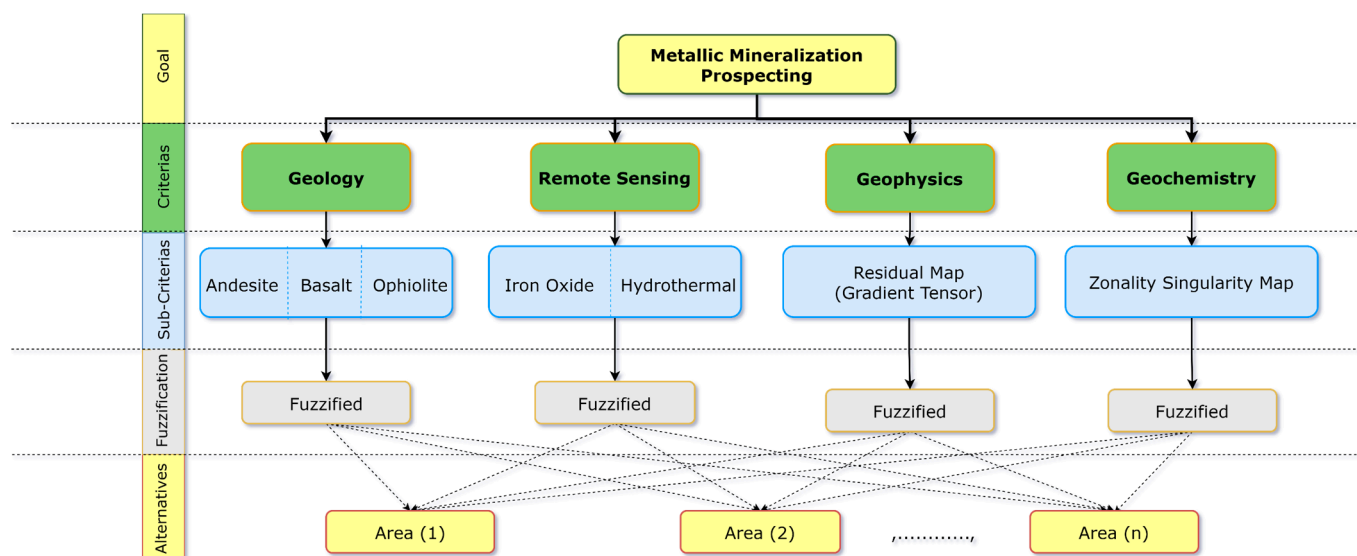


Figure 20. Hierarchical diagram of the fuzzy-AHP hybrid method and criteria and sub-criteria considered in decision making.

Table 5. Paired comparison matrix and the calculated weights of the main-criteria and sub-criteria by AHP method.

Main-Criteria Weighting						
	Geology	Geochemistry	Geophysics	Remote Sensing	Priority	Rank
Geology	1	0.33	2	1	17.90%	2
Geochemistry	3	1	7	3	55.70%	1
Geophysics	0.5	0.14	1	0.5	8.60%	3
Remote Sensing	1	0.33	2	1	17.90%	2
Sub-Criteria Weighting						
		Andesite	Basalt	Ophiolite	Priority	Rank
Geology	Andesite	1	1	6	46.20%	1
	Basalt	1	1	6	46.20%	1
	Ophiolite	0.17	0.17	1	7.70%	2
		Iron Oxide	Hydrothermal	Priority	Rank	
Remote Sensing	Fe Oxide	1	1	50.00%	1	
	Hydrothermal	1	1	50.00%	1	

At the fuzzification stage, all the information layers should be fuzzified according to fuzzy logic. The fuzzified layers are presented in Figure 21. Subsequently, these fuzzified layers are integrated based on calculated weights for all main-criteria and sub-criteria in the AHP method.

Figure 22 shows the metallic prospectivity map of the study area. As presented in the final prospectivity map, based on fuzzy logic, low potential areas are indicated with white to gray color and high potential areas tend to the black color.

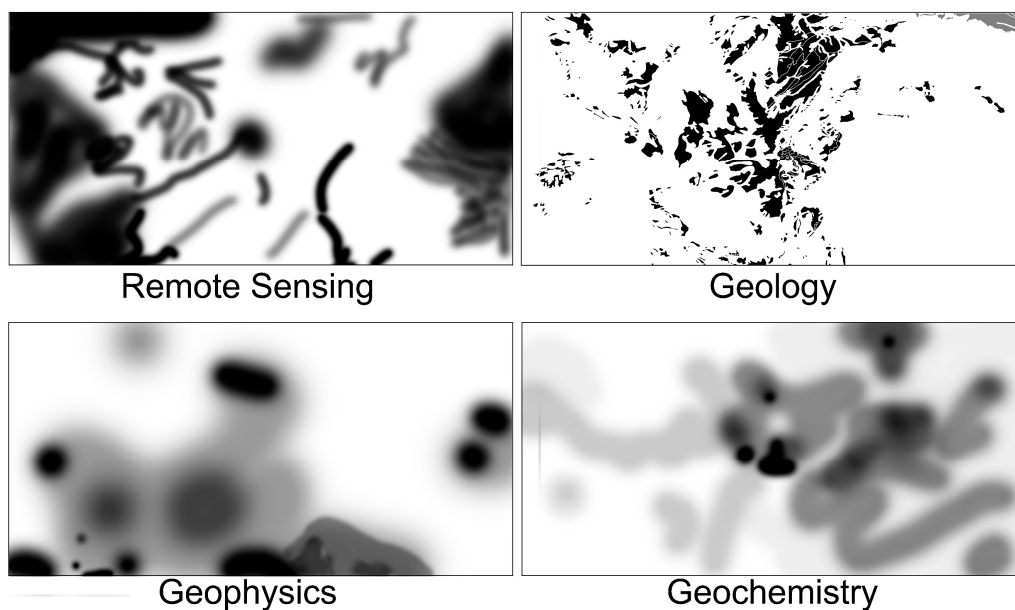


Figure 21. The fuzzified information layers for the study area.

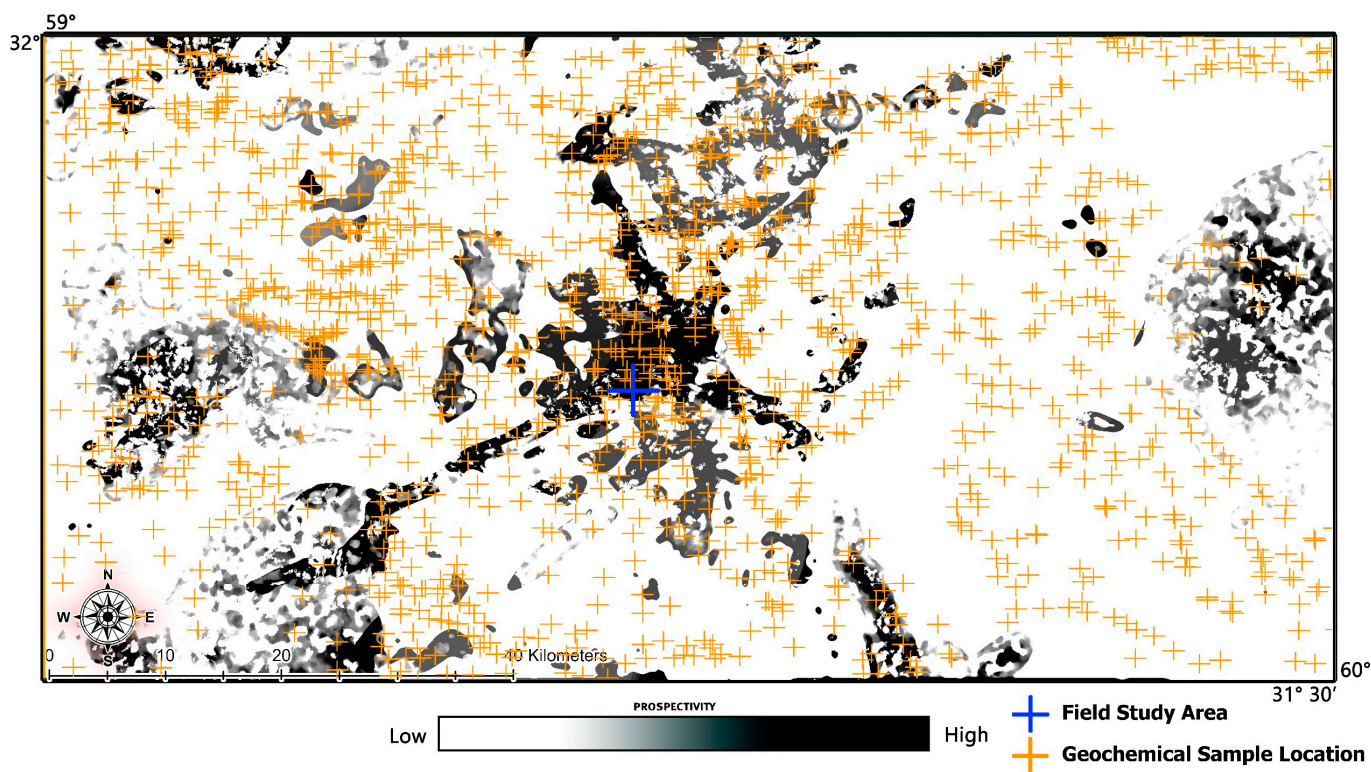


Figure 22. The metallic prospectivity map of the study area based on hybrid Fuzzy-AHP integrating method.

4.9. Fieldwork and Controlled Points

After the completion of analytical calculations and integration of information layers, some points were checked for validation of final metallic prospectivity map. A small area in the center of the study area was selected for laboratory studies and confirmation of the results. In total, six mineralogical samples, three petrological samples and three stream sediment samples, were collected for further studies. Microscopic mineralogical studies

confirmed the mineralization of malachite, pyrite, Fe hydroxides, and limonite. Microscopic images of polished sections prepared from the collected samples are presented in Figure 23.

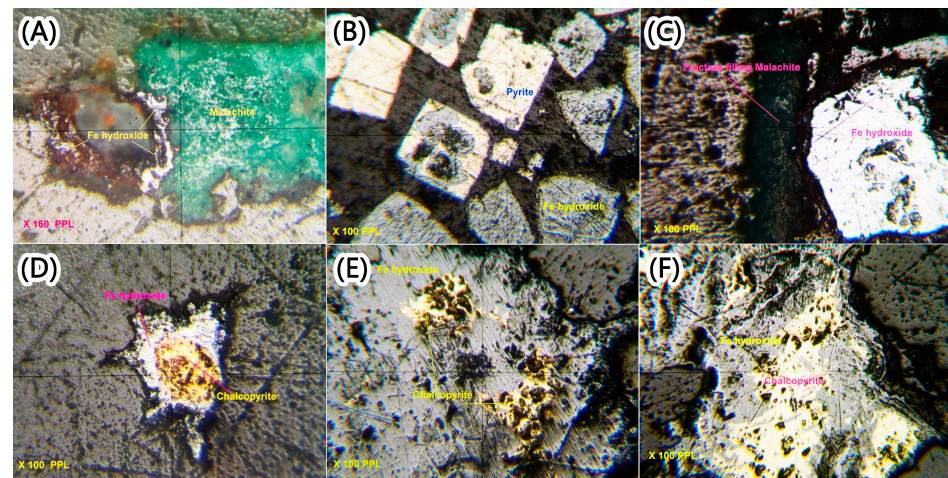


Figure 23. Polished sections of mineralogical samples from checked Points. (A) Malachite with Fe hydroxides in silica gangue; (B) Pyrite and Fe oxides, whose marginal parts have been replaced by limonite and goethite; (C) Fe hydroxides and malachite formed secondary along the fractures; (D) Chalcopyrite and Fe hydroxide in joints and fractures; (E) Chalcopyrite, most of which were replaced by Fe hydroxides due to supergene alteration; (F) Pyrite and chalcopyrite, limonite and goethite in the margins.

Based on petrographic studies of andesite-basalt samples, it was found that the section has plagioclase microlites that were completely replaced by argillaceous materials and clay minerals. Moreover, the basalt sample has clinopyroxene and plagioclase. The images (4× with natural light) related to the petrological study are presented in Figure 24A–C.

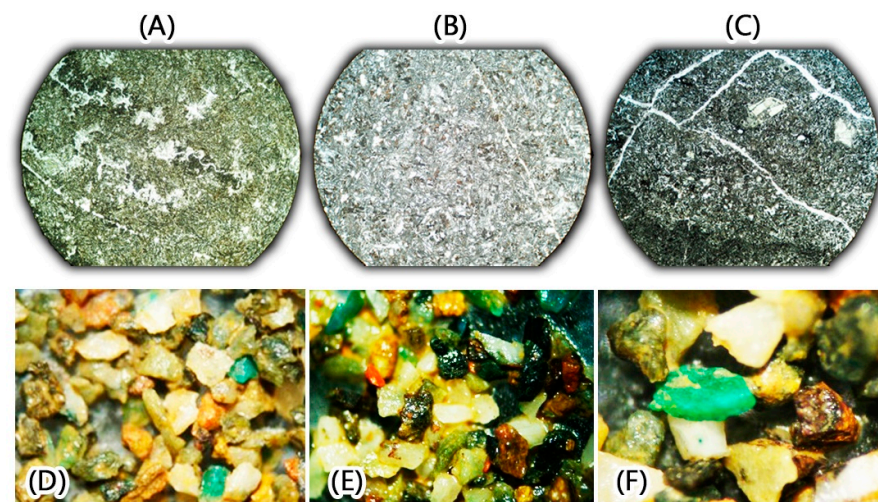


Figure 24. Petrological sections (4× magnification with natural light-A) and washed stream sediment samples (Binocular study (20×)). (A) Andesite-basalt, has plagioclase microlites that were completely replaced by argillaceous materials and clay minerals; (B) Basalt, contains clinopyroxene and plagioclase needles; (C) Andesite-basalt, containing plagioclase microlites from albite to oligoclase; (D) Malachite and a tiny amount of chalcopyrite; (E) Magnetite, quartz, calcite, limonite and olivine; (F) Malachite, quartz and limonite.

The stream sediment samples, whose binocular images are shown in Figure 24D–F, indicate that Cu oxide (malachite), magnetite, limonite, and chalcopyrite (in small amounts)

are present in the sediments. Moreover, non-metallic minerals, including quartz, calcite, and olivine, were identified.

5. Conclusions

The results of the present research provide support for metallic exploration with a special focus on Cu for reconnaissance stage in the Kodegan-Basiran region. The most important exploration keys are: (1) andesite, basalt, and ophiolite geological units as prospectivity host rock; (2) the map of hydrothermal alterations and iron oxides; (3) the location of intrusive masses based on aeromagnetic anomalies; (4) a geochemical anomalies map according to Pb, Zn, Bi, Ag, Mo, and Cu concentrations in the stream sediment samples; and (5) the integrated metallic prospectivity map obtained using the fuzzy-AHP. The mineralogical, petrological, and stream sediment samples from a control area showed metallic mineralization of Cu and Fe sulfides, oxides, and hydroxides.

Prospective areas which were introduced in the final integrated map, which can be targeted for Cu exploration in larger scales. Moreover, the results of this study will reduce financial and time costs of future exploratory studies. It is suggested that in order to increase the accuracy of reconnaissance studies, the density of geochemical sampling, geological and geophysical surveys in the high potential areas should be increased. In this way, the identified anomalies will be investigated more precisely.

Author Contributions: Conceptualization, A.S. (Ali Shabani), M.Z. and A.S. (Aref Shirazi); methodology, A.S. (Aref Shirazi), A.S. (Adel Shirazy), and A.S. (Ali Shabani); supervision, M.Z., M.S.M., A.S. (Adel Shirazy), and A.S. (Aref Shirazi). All authors have read and agreed to the published version of the manuscript.

Funding: This research received no external funding.

Data Availability Statement: Geochemical stream sediments and Geophysical Data are available on request from the Geological Survey of Iran (GSI). (www.GSI.ir).

Acknowledgments: We appreciate the assistance of the Faculty of Mining, Petroleum & Geophysics Engineering, Shahrood University of Technology. This study is part of the research activity carried out during the first author's Ph.D. research at the Faculty of Mining, Petroleum & Geophysics Engineering, Shahrood University of Technology. Amirkabir university of technology is also acknowledged for providing facilities for editing, rewriting, and re-organizing the manuscript. I would also like to thank the reviewers and academic editor of this article who helped to improve it effectively.

Conflicts of Interest: The authors declare no conflict of interest.

References

1. Shirmard, H.; Farahbakhsh, E.; Pour, A.B.; Muslim, A.M.; Müller, R.D.; Chandra, R. Integration of selective dimensionality reduction techniques for mineral exploration using ASTER satellite data. *Remote Sens.* **2020**, *12*, 1261. [[CrossRef](#)]
2. Parsa, M.; Maghsoudi, A. Assessing the effects of mineral systems-derived exploration targeting criteria for Random Forests-based predictive mapping of mineral prospectivity in Ahar-Arasbaran area, Iran. *Ore Geol. Rev.* **2021**, *138*, 104399. [[CrossRef](#)]
3. Bahrami, Y.; Hassani, H.; Maghsoudi, A. Spatial modeling for mineral prospectivity using BWM and COPRAS as a new HMCDM method. *Arab. J. Geosci.* **2022**, *15*, 394. [[CrossRef](#)]
4. Nafigin, I.O.; Ishmukhametova, V.T.; Ustinov, S.A.; Minaev, V.A.; Petrov, V.A. Geological and Mineralogical Mapping Based on Statistical Methods of Remote Sensing Data Processing of Landsat-8: A Case Study in the Southeastern Transbaikalia, Russia. *Sustainability* **2022**, *14*, 9242. [[CrossRef](#)]
5. Bencharef, M.H.; Eldosouky, A.M.; Zamzam, S.; Boubaya, D. Polymetallic mineralization prospectivity modelling using multi-geospatial data in logistic regression: The Diapiric Zone, Northeastern Algeria. *Geocarto Int.* **2022**, 1–36. [[CrossRef](#)]
6. Mahdi, A.M.; Eldosouky, A.M.; El Khateeb, S.O.; Youssef, A.M.; Saad, A.A. Integration of remote sensing and geophysical data for the extraction of hydrothermal alteration zones and lineaments; Gabal Shilman basement area, Southeastern Desert, Egypt. *J. Afr. Earth Sci.* **2022**, *194*, 104640. [[CrossRef](#)]
7. Ekwok, S.E.; Akpan, A.E.; Achadu, O.-I.M.; Thompson, C.E.; Eldosouky, A.M.; Abdelrahman, K.; András, P. Towards Understanding the Source of Brine Mineralization in Southeast Nigeria: Evidence from High-Resolution Airborne Magnetic and Gravity Data. *Minerals* **2022**, *12*, 146. [[CrossRef](#)]
8. Elkhateeb, S.O.; Eldosouky, A.M.; Khalifa, M.O.; Aboalhassan, M. Probability of mineral occurrence in the Southeast of Aswan area, Egypt, from the analysis of aeromagnetic data. *Arab. J. Geosci.* **2021**, *14*, 1514. [[CrossRef](#)]

9. Riahi, S.; Bahroudi, A.; Abedi, M.; Aslani, S.; Elyasi, G.-R. Integration of airborne geophysics and satellite imagery data for exploration targeting in porphyry Cu systems: Chahargonbad district, Iran. *Geophys. Prospect.* **2021**, *69*, 1116–1137. [[CrossRef](#)]
10. Riahi, S.; Bahroudi, A.; Abedi, M.; Aslani, S.; Elyasi, G. Evidential data integration to produce porphyry Cu prospectivity map, using a combination of knowledge and data-driven methods. *Geophys. Prospect.* **2022**, *70*, 421–437. [[CrossRef](#)]
11. Maleki, M.; Niroomand, S.; Rajabpour, S.; Pour, A.B.; Ebrahimpour, S. Targeting local orogenic gold mineralization zones using data-driven evidential belief functions: The Godarsorkh area, Central Iran. *All Earth* **2022**, *34*, 259–278. [[CrossRef](#)]
12. Ghorbani, M. The economic geology of Iran. In *Mineral Deposits and Natural Resources*; Springer: Berlin/Heidelberg, Germany, 2013; pp. 1–450.
13. Jung, D.; Keller, J.; Khorasani, R.; Marcks, C.; Baumann, A.; Horn, P. Petrology of the Tertiary magmatic activity in the northern Lut area, east of Iran. *Neues Jahrb. Für Geol. Und Paläontologie-Abh.* **1983**, *168*, 417–467. [[CrossRef](#)]
14. Samani, B.; Ashtari, S. Geological evolution of Sistan and Baluchestan area. *J. Earth Sci. Geol. Surv. Iran.* **1992**, *1*, 14–25.
15. Mehrabi, B.; Fazel, E.T.; Yardley, B. Ore geology, fluid inclusions and OS stable isotope characteristics of Shurab Sb-polymetallic vein deposit, eastern Iran. *Geochemistry* **2019**, *79*, 307–322. [[CrossRef](#)]
16. Ghorbani, M. Metallogenic and mining provinces, belts and zones of Iran. In *The Economic Geology of Iran*; Springer: Berlin/Heidelberg, Germany, 2013; pp. 199–295.
17. Samiee, S.; Karimpour, M.H. Gold Metallogeny in the East of Iran. *Period. Di Mineral.* **2022**, *91*. [[CrossRef](#)]
18. Shafaroudi, A.M.; Karimpour, M.H. Mineralogic, fluid inclusion, and sulfur isotope evidence for the genesis of Sechangi lead–zinc (–copper) deposit, Eastern Iran. *J. Afr. Earth Sci.* **2015**, *107*, 1–14. [[CrossRef](#)]
19. Karimpour, M.H.; Stern, C.; Malekzadeh, A.; Hidarian, M.; Mazaheri, A. Petrochemistry of the reduced, ilmenite-series granitoid intrusion related to the Hired gold-tin prospect (Basiran), Eastern Iran. *J. Appl. Sci.* **2009**, *9*, 226–236. [[CrossRef](#)]
20. Shafaroudi, A.M.; Karimpour, M.H. Geology, mineralization, and fluid inclusion studies of the Howz-e-Rais lead-zinc-copper deposit, Eastern Iran. *Adv. Appl. Geol.* **2012**, *2*, 63–73.
21. Aryafar, A.; Moeini, H.; Khosravi, V. CRFA-CRBM: A hybrid technique for anomaly recognition in regional geochemical exploration; case study: Dehsalm area, east of Iran. *Int. J. Min. Geo-Eng.* **2020**, *54*, 33–38.
22. Keykhay-Hosseinpoor, M.; Kohsary, A.H.; Hossein-Morshedy, A.; Porwal, A. A machine learning-based approach to exploration targeting of porphyry Cu-Au deposits in the Dehsalm district, eastern Iran. *Ore Geol. Rev.* **2020**, *116*, 103234. [[CrossRef](#)]
23. Arjmandzadeh, R.; Santos, J. Sr–Nd isotope geochemistry and tectonomagmatic setting of the Dehsalm Cu–Mo porphyry mineralizing intrusives from Lut Block, eastern Iran. *Int. J. Earth Sci.* **2014**, *103*, 123–140. [[CrossRef](#)]
24. Shirazi, A.; Hezarkhani, A.; Pour, A.B. Fusion of Lineament Factor (LF) Map Analysis and Multifractal Technique for Massive Sulfide Copper Exploration: The Sahlabad Area, East Iran. *Minerals* **2022**, *12*, 549. [[CrossRef](#)]
25. Khosravi, V.; Shirazi, A.; Shirazy, A.; Hezarkhani, A.; Pour, A.B. Hybrid Fuzzy-Analytic Hierarchy Process (AHP) Model for Porphyry Copper Prospecting in Simorgh Area, Eastern Lut Block of Iran. *Mining* **2021**, *2*, 1–12. [[CrossRef](#)]
26. Bai, H.; Cao, Y.; Zhang, H.; Zhang, C.; Hou, S.; Wang, W. Combining fuzzy analytic hierarchy process with concentration–area fractal for mineral prospectivity mapping: A case study involving Qinling orogenic belt in central China. *Appl. Geochem.* **2021**, *126*, 104894. [[CrossRef](#)]
27. Kharbish, S.; Eldosouky, A.M.; Amer, O. Integrating mineralogy, geochemistry and aeromagnetic data for detecting Fe–Ti ore deposits bearing layered mafic intrusion, Akab El-Negum, Eastern Desert, Egypt. *Sci. Rep.* **2022**, *12*, 1–19. [[CrossRef](#)] [[PubMed](#)]
28. Iran, G.S.I. *Basiran 1:100,000 Geological Map*; GSI: Tehran, Iran, 1992.
29. Iran, G.S.I. *Koudakan 1:100,000 Geological Map*; GSI: Tehran, Iran, 1993.
30. Karimpour, M.H.; Stern, C.; Farmer, L.; Saadat, S. Review of age, Rb–Sr geochemistry and petrogenesis of Jurassic to Quaternary igneous rocks in Lut Block, Eastern Iran. *Geopersia* **2011**, *1*, 19–54.
31. Moghaddam, M.J.; Karimpour, M.H.; Shafaroudi, A.M.; Santos, J.F.; Corfu, F. Middle Eocene magmatism in the Khur region (Lut Block, Eastern Iran): Implications for petrogenesis and tectonic setting. *Int. Geol. Rev.* **2021**, *63*, 1051–1066. [[CrossRef](#)]
32. Maghfouri, S.; Hosseinzadeh, M.R.; Lentz, D.R.; Tajeddin, H.A.; Movahednia, M.; Shariefi, A. Nature of ore-forming fluids in the Mehdiabad world-class sub-seafloor replacement SEDEX-type Zn–Pb–Ba–(Cu–Ag) deposit, Iran; constraints from geochemistry, fluid inclusions, and OC–Sr isotopes. *J. Asian Earth Sci.* **2021**, *207*, 104654. [[CrossRef](#)]
33. Nejad, A.T.; Khalaji, A.A.; Ebrahimi, M.; Biabangard, H.; Esmaeili, R. Petrology, geochemistry, source and tectonic setting of Malek Chah Ruii granitoid (East of Lut Block). *Iran. J. Petrol.* **2021**, *12*, 63–92.
34. Ghorbani, M. A summary of geology of Iran. In *The Economic Geology of Iran*; Springer: Berlin/Heidelberg, Germany, 2013; pp. 45–64.
35. Iran, G.S. *Geochemical Map Report for Basiran and Kodegan 1:100,000 Map*; GSI: Tehran, Iran, 1992.
36. Shirazi, A.; Hezarkhani, A.; Pour, A.B.; Shirazy, A.; Hashim, M. Neuro-Fuzzy-AHP (NFAHP) Technique for Copper Exploration Using Advanced Spaceborne Thermal Emission and Reflection Radiometer (ASTER) and Geological Datasets in the Sahlabad Mining Area, East Iran. *Remote Sens.* **2022**, *14*, 5562. [[CrossRef](#)]
37. Aliabad, F.A.; Shojaei, S.; Zare, M.; Ekhtesasi, M.R. Assessment of the fuzzy ARTMAP neural network method performance in geological mapping using satellite images and Boolean logic. *Int. J. Environ. Sci. Technol.* **2019**, *16*, 3829–3838. [[CrossRef](#)]
38. Ahmadi, H.; Uygucgil, H. Targeting iron prospective within the Kabul Block (SE Afghanistan) via hydrothermal alteration mapping using remote sensing techniques. *Arab. J. Geosci.* **2021**, *14*, 183. [[CrossRef](#)]

39. Shirazi, A.; Hezarkhani, A.; Shirazy, A. Remote sensing studies for mapping of iron oxide regions, South of Kerman, Iran. *Int. J. Sci. Eng. Appl.* **2018**, *7*, 45–51. [[CrossRef](#)]
40. Esmaeili, J.; Khakzad, A.; Abedini, M.V. Integration and analysis of geology data and Remote sensing methods for identification and separate of alternations iron ore of kamoo (Meymeh-Isfahan). *Sci. Q. J. Geosci.* **2020**, *29*, 15–22.
41. Shirazy, A.; Hezarkhani, A.; Timkin, T.; Shirazi, A. Investigation of Magneto-/Radio-Metric Behavior in Order to Identify an Estimator Model Using K-Means Clustering and Artificial Neural Network (ANN) (Iron Ore Deposit, Yazd, IRAN). *Minerals* **2021**, *11*, 1304. [[CrossRef](#)]
42. Safronov, N. Dispersion haloes of ore deposits and their use in exploration. *Probl. Sov. Geol.* **1936**, *4*, 41–53.
43. Carranza, E.J.M. Primary geochemical characteristics of mineral deposits: Implications for exploration. *Ore Geol. Rev.* **2012**, *45*, 1–4. [[CrossRef](#)]
44. Ziaii, M. Litho-geochemical Exploration Methods for Porphyry Copper Deposit in Sungun, NW Iran. Master's Thesis, Moscow State University (MSU), Moscow, Russia, 1996; p. 98.
45. Safari, S.; Ziaii, M.; Ghoorchi, M. Integration of singularity and zonality methods for prospectivity map of blind mineralization. *Int. J. Min. Geo-Eng.* **2016**, *50*, 189–194.
46. Likas, A.; Vlassis, N.; Verbeek, J.J. The global k-means clustering algorithm. *Pattern Recognit.* **2003**, *36*, 451–461. [[CrossRef](#)]
47. Saha, S.; Bandyopadhyay, S. A generalized automatic clustering algorithm in a multiobjective framework. *Appl. Soft Comput.* **2013**, *13*, 89–108. [[CrossRef](#)]
48. Hezarkhani, A.; Ghannadpour, S.S. *Geochemical Behavior Investigation Based on K-Means Clustering: Basics, Concepts and Case Study*; LAP LAMBERT Academic Publishing: Saarbrücken, Germany, 2015.
49. Shirazi, A.; Shirazy, A.; Saki, S.; Hezarkhani, A. Introducing a software for innovative neuro-fuzzy clustering method named NFCMR. *Glob. J. Comput. Sci. Theory Res.* **2018**, *8*, 62–69. [[CrossRef](#)]
50. Shirazy, A.; Shirazi, A.; Hezarkhani, A. *Behavioral Analysis of Geochemical Elements in Mineral Exploration: Methodology and Case Study*; LAP LAMBERT Academic Publishing: Saarbrücken, Germany, 2020.
51. Chen, L.; Guan, Q.; Feng, B.; Yue, H.; Wang, J.; Zhang, F. A multi-convolutional autoencoder approach to multivariate geochemical anomaly recognition. *Minerals* **2019**, *9*, 270. [[CrossRef](#)]
52. Rantitsch, G. The fractal properties of geochemical landscapes as an indicator of weathering and transport processes within the Eastern Alps. *J. Geochem. Explor.* **2001**, *73*, 27–42. [[CrossRef](#)]
53. Nazarpour, A. Application of CA fractal model and exploratory data analysis (EDA) to delineate geochemical anomalies in the Takab 1: 25,000 geochemical sheet, NW Iran. *Iran. J. Earth Sci.* **2018**, *10*, 173–180.
54. Shuguang, Z.; Kefa, Z.; Yao, C.; Jinlin, W.; Jianli, D. Exploratory data analysis and singularity mapping in geochemical anomaly identification in Karamay, Xinjiang, China. *J. Geochem. Explor.* **2015**, *154*, 171–179. [[CrossRef](#)]
55. Zuo, R.; Xia, Q.; Zhang, D. A comparison study of the C–A and S–A models with singularity analysis to identify geochemical anomalies in covered areas. *Appl. Geochem.* **2013**, *33*, 165–172. [[CrossRef](#)]
56. Zuo, R.; Wang, J.; Chen, G.; Yang, M. Identification of weak anomalies: A multifractal perspective. *J. Geochem. Explor.* **2015**, *148*, 12–24. [[CrossRef](#)]
57. Liu, Y.; Xia, Q.; Cheng, Q.; Wang, X. Application of singularity theory and logistic regression model for tungsten polymetallic potential mapping. *Nonlinear Process. Geophys.* **2013**, *20*, 445–453. [[CrossRef](#)]
58. Turcotte, D.L. *Fractals and Chaos in Geology and Geophysics*, 2nd ed.; Cornell University: New York, NY, USA, 1997.
59. Zuo, R.; Cheng, Q.; Agterberg, F.; Xia, Q. Application of singularity mapping technique to identify local anomalies using stream sediment geochemical data, a case study from Gangdese, Tibet, western China. *J. Geochem. Explor.* **2009**, *101*, 225–235. [[CrossRef](#)]
60. Khan, S.A.; Naim, I.; Kusi-Sarpong, S.; Gupta, H.; Idrisi, A.R. A knowledge-based experts' system for evaluation of digital supply chain readiness. *Knowl.-Based Syst.* **2021**, *228*, 107262. [[CrossRef](#)]
61. Wang, C.-N.; Nguyen, N.-A.; Dang, T.-T.; Lu, C.-M.A. A compromised decision-making approach to third-party logistics selection in sustainable supply chain using fuzzy AHP and fuzzy VIKOR methods. *Mathematics* **2021**, *9*, 886. [[CrossRef](#)]
62. Padma, T.; Shantharajah, S.; Ramadoss, P. Hybrid Fuzzy AHP and Fuzzy TOPSIS Decision Model for Aquaculture Species Selection. *Int. J. Inf. Technol. Decis. Mak.* **2022**, *21*, 999–1030. [[CrossRef](#)]
63. Shirazy, A.; Shirazi, A.; Heidarlaki, S.; Ziaii, M. Exploratory Remote Sensing Studies to Determine the Mineralization Zones around the Zarshuran Gold Mine. *Int. J. Sci. Eng. Appl.* **2018**, *7*, 274–279. [[CrossRef](#)]
64. Payamani, A.; Babaei, B.; Dehghan, S.; Harouni, H.A. Applying various satellite image processing methods on Aster and Landsat ETM+ data to identify and separate the alteration zones around gold mine of Akhtarchi, Khomein, Iran. *Nexo Rev. Científica* **2020**, *33*, 490–510. [[CrossRef](#)]
65. Ziaii, M.; Carranza, E.J.M.; Ziaei, M. Application of geochemical zonality coefficients in mineral prospectivity mapping. *Comput. Geosci.* **2011**, *37*, 1935–1945. [[CrossRef](#)]
66. Shirazi, A.; Shirazy, A.; Karami, J. Remote sensing to identify copper alterations and promising regions, Sarbishe, South Khorasan, Iran. *Int. J. Geol. Earth Sci.* **2018**, *4*, 36–52.
67. Shirazy, A.; Hezarkhani, A.; Shirazi, A.; Khakmardan, S.; Rooki, R. K-Means Clustering and General Regression Neural Network Methods for Copper Mineralization probability in Chahar-Farsakh, Iran. *Türkiye Jeol. Bülteni* **2022**, *65*, 79–92.
68. Shirazy, A. Investigation of Geochemical Sections in Exploratory Boreholes of Mesgaran Copper Deposit in Iran. *Int. J. Res. Appl. Sci. Eng. Technol.* **2021**, *9*, 2364–2368. [[CrossRef](#)]

69. Alahgholi, S.; Shirazy, A.; Shirazi, A. Geostatistical studies and anomalous elements detection, Bardaskan Area, Iran. *Open J. Geol.* **2018**, *8*, 697–710. [[CrossRef](#)]
70. Shirazy, A.; Hezarkhani, A.; Shirazy, A.; Timkin, T.V.; Voroshilov, V.G. Geophysical explorations by resistivity and induced polarization methods for the copper deposit, South Khorasan, Iran. *Bull. Tomsk. Polytech. Univ. Geo Assets Eng.* **2022**, *333*, 99–110. [[CrossRef](#)]
71. Aali, A.A.; Shirazy, A.; Shirazi, A.; Pour, A.B.; Hezarkhani, A.; Maghsoudi, A.; Hashim, M.; Khakmardan, S. Fusion of Remote Sensing, Magnetometric, and Geological Data to Identify Polymetallic Mineral Potential Zones in Chakchak Region, Yazd, Iran. *Remote Sens.* **2022**, *14*, 6018. [[CrossRef](#)]
72. Saaty, T.L. *Fundamentals of Decision Making and Priority with the AHP*; RWS Publications: Pittsbergh, PA, USA, 1994.
73. Goepel, K.D. Implementation of an online software tool for the analytic hierarchy process (AHP-OS). *Int. J. Anal. Hierarchy Process* **2018**, *10*, 469–487.